
University of Stuttgart
Institute for Control Engineering
of Machine Tools and Manufacturing Units
(ISW)

Master's Thesis

SLOG: Single Label Object Grasping

submitted by

Kanishk Umesh Navale

from India

Degree program	M. Sc. Computer Science
Examined by	Prof. Andreas Wortmann
Supervised by	Mr. Tobius Bux
Submitted on	31 October 2022

Declaration of Originality

Master's Thesis of Kanishk Umesh Navale (M. Sc. Computer Science)

Address	Allmandring 22A-10, 70569 Stuttgart
Student number	3437531
English title	*SLOG: Single Label Object Grasping*
German title	*Einklassige verallgemeinerte visuelle Einbettung von Objektpunkten für das Greifen von Robotern*

I now declare,

- that I wrote this work independently,
- that no sources other than those stated are used and that all statements taken from other works—direcly or figuratively—are marked as such,
- that the work submitted was not the subject of any other examination procedure, either in its entirety or in substantial parts,
- that I have not published the work in whole or in part, and
- that my work does not violate any rights of third parties and that I excempt the University against any claims of third parties.

Stuttgart, 31 October 2022

Kurzfassung

In dieser Arbeit wird ein Rahmenwerk für künstliche Intelligenz vorgeschlagen, um eine verallgemeinerte visuelle Objektdarstellung für Roboter-Greifaufgaben zu entwickeln.

Ein einzelnes Label wird aus der verallgemeinerten visuellen Objektdarstellung extrahiert, um ein Objekt auf einer pixelbasierten Skala zu identifizieren, das dann als Greifpunkt für einen Roboter dient. Die verallgemeinerten visuellen Objektdarstellungen, die aus Dense Object Nets (DON) berechnet werden, werden zur Berechnung der 6D-Position von Objekten verwendet, um eine robuste Roboter-Greifpipeline zu erstellen. Um die Notwendigkeit einer manuellen Extraktion von Beschriftungen aus den von DON berechneten Repräsentationen zu eliminieren, wird KeypointNet implementiert. Die Pipeline für die semantische Objektkorrespondenz wurde auf der Grundlage der Generalisierungsfähigkeiten des KeypointNet entwickelt, um DON weiter zu trainieren. Gleichzeitig haben wir festgestellt, dass das KeypointNet für sich genommen bereits die Fähigkeit besitzt, verallgemeinerte visuelle Objektrepräsentationen ähnlich wie DON zu berechnen, was den Gedanken nahelegt, dass es auch andere Netzwerke gibt, die in der Lage sind, verallgemeinernde Merkmale zu erzeugen.

Im Kern demonstriert diese Arbeit die eingeschränkten Fähigkeiten von Netzwerken für die Erzeugung verallgemeinerten visuellen Objektdarstellungen, wenn sie nur auf dem synthetischen Datensatz trainiert werden.

Im Gegensatz zum isolierten KeypointNet konnten wir für das KeypointNet Robustheit gegenüber Objektverdeckungen im Blickpunkt erreichen, wenn es auf DON-Darstellungen in einer End-to-End-Methode trainiert wurde. Darüber hinaus wählt das KeypointNet, das mit den von DON berechneten Repräsentationen arbeitet, selbstständig einzelne Labels aus und berechnet geometrisch konsistente 6D-Posen für semantisch ähnliche Objekte. Abschließend wird die Robustheit des objektgeneralisierenden Frameworks bei der Generalisierung von realen Kappen und Manipulationen anhand eines realen Robotermanipulators demonstriert.

Stichwörter: Künstliche Intelligenz, verallgemeinerte visuelle Objektrepräsentationen, DON, KeypointNet, geometrisch konsistente Keypoints, semantische Objektkorrespondenz-Pipeline, DON-Informiertes KeypointNet, Ende-zu-Ende-Training von neuronalen Netzen, synthetischer Datensatz, robuste 6D-Objektposen, Eizelnlabel-Objekgreifen, Demonstration von Roboteraufgaben

Abstract

The thesis proposes an artificial intelligence framework to develop generalized visual object representation for robot grasping tasks.

A single label is extracted from the generalized visual object representation to identify an object on a pixel-wise scale, acting as a robot grasping point. The generalized visual object representations computed from DON are applied to compute objects' 6D pose to create a robust robot grasping pipeline. To eliminate the need for the manual label extraction from the representations computed by DON, KeypointNet is implemented. The semantic object correspondence pipeline is engineered based on generalizing capabilities of the KeypointNet to train DON further. At the same time, the thesis identified that the KeypointNet on its own already demonstrates the capabilities of computing generalized visual object representation similar to DON, ushering the idea that there are other networks capable of generalizing features.

At its core, this thesis demonstrates the reduced capabilities of networks to produce generalized visual object representation when only trained on the synthetic dataset.

In contrast to KeypointNet training in isolation, the thesis could achieve robustness for the KeypointNet against the object occlusions in viewpoint when trained on DON representations in an end-to-end fashion. Furthermore, the KeypointNet trained with DON representations autonomously picks single class generalized labels. Additionally, computing geometrically consistent 6D poses across semantically similar objects.

Finally, the proposed framework demonstrates robustness in generalizing real-world caps and manipulation by employing a real-world robot manipulator.

Keywords: artificial intelligence, generalized visual object representations, DON, KeypointNet, geometrically consistent keypoints, semantic object correspondence pipeline, DON Informed KeypointNet, end-to-end neural network training, synthetic dataset, robust object 6D poses, single label object grasping, robot task demonstration

Acknowledgement

I want to thank the entire `sereact` [1] team for their tremendous support and guidance throughout the completion of this thesis. Furthermore, I thank Olga Klimashevska (Olgsy) and Nirbhay Jain (Bablu) for their valuable input.

Contents

Kurzfassung ii

Abstract iii

Acknowledgment iv

1 Introduction 1
1.1 Motivation . . . 2

2 State of the Art 5
2.1 Overview . . . 5
2.2 Breakdown Analysis & Comparison of Influential State of the Art (SOTA) 8

3 Objective 12

4 Methodology 13
4.1 Dense Object Nets . . . 13
4.1.1 Implementation Strategy . . . 14
4.1.2 ResNet Architectures . . . 14
4.1.3 Loss Functions . . . 14
4.1.4 *PCK@k* as an Evaluation Metric . . . 17
4.1.5 Suzanne, a synthetic dataset . . . 17
4.1.6 Manual Method for Robot Grasp Generation . . . 18
4.2 KeypointNet . . . 19
4.2.1 Loss functions . . . 19
4.2.2 Total Weighted-Sum Loss . . . 23
4.2.3 Network Modification . . . 24
4.3 End-to-End Network Training . . . 24
4.3.1 KeypointNet Informed Dense Object Nets . . . 24
4.3.2 Dense Object Nets Informed KeypointNet . . . 25
4.3.3 Mining Dense Object Nets Representations in KeypointNet . . . 25
4.4 Generalizing "Caps" . . . 26
4.4.1 Semantic Correspondences Mapping Pipeline . . . 27
4.4.2 Tweaking the Training Pipeline . . . 27
4.4.3 Evaluating Single Class Generalized Labels in the Wild . . . 28
4.4.4 Robot Grasping Pipeline . . . 28

5 Results **30**
5.1 Dense Object Nets 30
5.1.1 Manual Method for Robot Grasp Generation 31
5.2 KeypointNet 32
5.3 End-to-End Training 33
5.3.1 KeypointNet Informed Dense Object Nets 33
5.3.2 Dense Object Nets Informed KeypointNet 33
5.3.3 Mining Dense Object Nets Representations in KeypointNet 34
5.4 Generalizing "Caps" 35
5.4.1 Semantic Correspondence Mapping Pipeline 35
5.4.2 Evaluating Single Class Generalized Labels in the Wild 36
5.4.3 *"Not losing hope on the real world"* 39
5.4.4 Robot Grasping Pipeline 40

6 Conclusion **42**

7 Future Scope **44**

Bibliography **45**

List of Acronyms **50**

List of Figures **51**

List of Tables **52**

Listings **53**

List of Symbols **54**

1 Introduction

Creating a general-purpose robot that can carry out practical activities, like Chappie or C-3PO, is one of the objectives of robotics in general and robotic manipulation in particular. Even if advancements toward this objective have been made recently in adjacent domains, it is still a work in progress. E.g., AlphaGo [2], a gameplaying artificial intelligence system trained entirely on self-play, defeated Lee Sedong, the world's best human Go player at the time. Subsequently, Silver *et al.* [3], developed artificial intelligence algorithms mastering the game of chess, Go, World of Warcraft and Shogi, surpassing human playing expertise. Most of these algorithms learn by drawing understanding directly from visual data such as gameplay recordings or online video streams emphasizing that the visual data is essential.

Meanwhile, the launch of AlexNet [4] in 2012 transformed the realm of computer vision. Other visual tasks, such as semantic segmentation [5], object identification and recognition [6], and human posture estimation [7], witnessed significant gains in the years that followed. Robotics has also made significant breakthroughs, ranging from self-driving cars to humanoid robots capable of performing remarkably active jobs recently developed using camera and other vision sensors.

Despite these advancements, the most frequently used robotic manipulation systems haven't evolved much in the previous 30 years. Typical auto-factory robots continue to do repetitive operations such as welding and painting, with the robot following a pre-programmed course with no feedback from the surroundings. If we want to increase the utility of our robots, we must move away from highly controlled settings and robots that do repetitive actions with little feedback or adaptability capabilities. Liberating ourselves from these restraints of controlled settings based manufacturing would allow us to enter new markets, as witnessed by the proliferation of firms [1] competing in the logistics domain.

In this thesis, we want to take things further by providing a generalized approach for vision-based robot tasks in real-world contexts. We employ a combination of classical robotics, computer vision and current deep-learning methods. While there are lessons to be drawn from deep learning, artificial intelligence and computer vision breakthroughs, we highlight the particular problems of machine vision based problems in robot manipulation. We offer an innovative generalized approach to address them.

1.1 Motivation

As of this writing, the ideal object representation for robot grasping and manipulation tasks is yet unknown. The existing representations may not be the best for tackling more complex tasks as they lack actual object information belonging to the same class and configuration (shape, color and size).

In industrial robot-based automation, the objects are specifically coded for their visual features using 2D and 3D vision systems. The downside of this lies in the fact that the robot has to be taught to pick every other part with its visual representation. This process comes with the tedious schedule of teaching the robot to pick every part irrespective of the part's configuration, and viewpoint. The solution lies in using artificial intelligence powered robots.

With so much focus on modern artificial intelligence, it is easy to overlook that the topic is not new. Artificial intelligence has undergone several phases, each defined by whether the emphasis was on proving logical theorems or attempting to emulate the human mind through neurology.

Artificial intelligence may be traced back to the late 1950s when computer pioneers such as Alan Turing and John von Neumann began investigating how machines might "think"[8]. However, a watershed moment in artificial intelligence happened in 1957, when researchers demonstrated that if given an infinite amount of memory, a machine could answer any issue.

The development of artificial intelligence made great strides in the 21st century. The first significant breakthrough was the creation of the self-learning neural network. By 2001, it had already outperformed humans in several domains, including object categorization and machine translation. Researchers enhanced its performance across a wide range of tasks over the following few years, thanks to advancements in the underlying technology. To a great extent artificial intelligence is empowered by machine learning and by Deep Learning (DL) in particular. Machine learning enables computers to learn from data and experience in order to enhance their performance on certain tasks or decision-making processes. For this reason, machine learning employs statistics and probability theory. Furthermore, machine learning employs algorithms to read data, learn from it, and make decisions without the need for explicit programming. Machine learning algorithms are frequently classified as either supervised or unsupervised. Supervised algorithms may apply previous learning to new data sets, whereas unsupervised algorithms can derive conclusions from datasets. Additionally, machine learning algorithms are programmed to seek out linear and non-linear correlations in a set of data. The learning is accomplished by the application of statistical approaches to train the

algorithm to categorize or predict from a dataset.

DL extends machine learning using multi-layered artificial neural networks, i.e., the so-called Deep Neural Network (DNN) to achieve cutting-edge accuracy in object detection, speech recognition, and language translation. DNN is a critical technology underlying autonomous automobiles because it allows machines to analyze enormous volumes of complicated data in real-time, such as identifying people's faces in an image or video.

Artifical neural networks are based on biological neurons in the human brain and are made up of layers of linked nodes called "neurons" that include mathematical functions to analyze incoming input and anticipate an output value. Similar to how we learn from our parents, instructors, and peers, artificial neural networks learn by examples (datasets). Deep learning models performance continues to increase as more data is added.

A Convolutional Neural Network (CNN) is a DNN that is designed to pick up features and patterns in structural data such as images. For example, having an extensive collection of object photos with more information such as depth and camera poses, CNN will easily learn the task-specific visual features. Furthermore, with task-specific optimizations, CNN can transform objects' visual features.

These CNN capabilities have enabled robots with skills to identify a part on an industrial fixture or in a bin since the networks have learned to recognise these parts from a series of images of these parts and other related visual data. If a new unseen part is in the bin, then the CNN is on the verge of object detection failure halting the robot cell in production or increasing the frequency of bin changing due to unpicked parts, which is an unfavorable industrial situation.

One of the ways to address this issue is by training a CNN to predict or regress a center point on an object silhoutte which would then serve as a robot gripping point. This prediction is bound to fail when the object is of a complex or non-convex shape resulting in misalignment and subsequently in robot grasping failure. In such a case, the neural networks are additionally trained to predict the object pose. These joint predictions of object recognition and its pose are often computationally costly resulting in increase of the robot system engineering costs to meet the production goals.

We are now coming to an understanding that the two significant problems involve robot teaching for all the objects and in which orientation the robot has to pick the object.

Florence *et al.* [9] introduced a novel visual object representation to the robotics community, terming it "dense object descriptors". The dense object descriptors could generalize

an object up to a certain extent and have been recently applied to rope manipulation [10], block manipulation [11], robot control [12], fabric manipulation [13] and robot grasp pose estimation [14]. This prior research lays one of the solid foundations for this thesis for object generalization.

The next area of this thesis is to encompass the dense object descriptors-based representations with 6D-Pose [1] information about the object. Given a particular photograph of an object with its depth map (together RGB-D data) and its camera relative position, the photograph pixels can be converted to a set of 3D points or pointcloud [15]. The object pointcloud can be sampled using various methodologies [16, 17]. The obtained object pointcloud can be transformed into a 6D-Pose using Principal Component Analysis (PCA) [18] or Singular Value Decomposition (SVD) [19] methods. Meanwhile, DNN can be trained for multiple tasks [20]. We can, thus, adopt PCA or SVD methodologies to train the neural network to predict dense object descriptors with object poses while the DNN learns and embed both the task information.

If the object is occluded, then the pose associated with it changes causing robot grasping failure. Suwajanakorn *et al.* [21] introduced a method to train CNN for pose reconstruction based on geometrically consistent keypoints, i.e., a point that carries certain (predefined) properties. One of the advantages is that when the object is occluded, the network can recall the hidden keypoints in the occlusion. This way, such a network is still able to reconstruct object pose from which one can now compute robot grasping pose consistently.

[1] 6D-Pose of an object refers to the object position and rotation in a 3D space.

2 State of the Art

The term "state of the art" refers to the most advanced degree of development accomplished in a design, method, material, or technology. It is an important consideration in any engineering feat. The overview section focuses on recent developments in the machine vision field that generalize object representations for robot grasping.

2.1 Overview

In 2017, Schmidt *et al.* [22] introduced instance-level generalization of objects using dense object descriptors. The dense object descriptors are embeddings for pixels in an image such that all pixels are uniquely defined with respect to each other. Specifically, Schmidt *et al.* [22] could generalize a human body pose with sequenced RGB-D data with mutual temporal correspondence using Scale-Invariant Feature Transform (SIFT) [23]. In this case, the dense object descriptors are computed using non-linear functions ($f : I_{RGB}[u, v] \in \mathbb{R}^3 \rightarrow I_D[u, v] \in \mathbb{R}^D$) converting an image pixel to an arbitrary vector of length $D \in \mathbb{N}^+$. Based on the adaptation of previously introduced non-linear function popularly known as the constrastive loss [24], "Pixelwise Contrastive Loss" is introduced by Florence *et al.* [9]. Florence *et al.* [9] introduced DON which is a self-supervised network that converts an 3-Channel Image (RGB) picture into a descriptor space image that implicitly stores essential object features invariant to the viewpoint, configuration and illumination. DON's self-supervised training is impressive in terms of speed in training and generalization. We can apply it to random objects and deploy it in half an hour [9]. Furthermore, DON learns from correspondences in an image pair.

In detail, the DON converts every pixel ($I[u, v] \in \mathbb{R}^3$) in the RGB image to a higher dimensional embedding ($I_D[u, v] \in \mathbb{R}^D$). In the field of machine learning or data engineering, embeddings are often applied for data dimensionality reduction, i.e., reducing the number of data features to a lower feature space. A lower-dimensional data space computed from a higher-dimension space uses embeddings to preserve the Euclidean distance of the dataspace [25]. In the case of the data dimensionality reduction, the embeddings preserve the linear distance in the data for reduction. The embeddings can be generated based on any property. For non-linear data dimensionality reduction, T-SNE [26] and Laplacian Eigenmaps [27] construct embeddings based on different properties in the data. Meanwhile, the higher dimension embedding computed from DON as dense descriptors captures and embeds information for viewpoint invariance,

illumination changes and object configuration from a sequence of images.

The DON training strategy relies on the depth information for computing correspondences in an image pair using camera intrinsics and pose information [28]. However, when employing consumer-grade depth cameras for capturing the depth information, the depth cameras capture noisy depth in cases of tiny, reflecting objects, which are common in industrial environments. In the meantime, Kupcsik *et al.* [14] used Laplacian Eigenmaps [27] to embed a 3D object model into an optimally generated embedding space acting as an target to train DON in a supervised fashion. The optimal embeddings brings in more domain knowledge by associating 3D object model to images views. Kupcsik *et al.* efficiently apply it to smaller, texture-less and reflective objects by eliminating the need of the depth information. Kupcsik *et al.* [14] further compare training strategies for producing 6D grasps for industrial objects and show that a unique supervised training approach increases pick-and-place resilience in industry-relevant tasks.

Differently, Hadjivelichkov and Kanoulas [29] extends the DON training using semantic correspondences between objects in multi-object or cluttered scenes overcoming the limitations of [28, 27]. The authors, Hadjivelichkov and Kanoulas [29] employ offline unsupervised clustering based on confidence in object similarities to generate hard and soft correspondence labels. The computed hard and soft labels lead DON in learning class-aware dense object descriptors, introducing hard and soft margin constraints in the proposed pixelwise contrastive loss.

Florence [30] has found that the pixelwise contrastive loss function used to train DON might not perform well if a computed correspondence is spatially inconsistent (analogously to the case of noisy depth information). This further highlights that the precision of contrastive-trained models can be sensitive to the relative weighting between positive-negative sampled pixels. Instead, the Florence [30] introduces a new continuous sampling-based loss function called "Pixelwise Distribution Loss". The pixelwise distribution loss is much more effective as it is a smooth continuous pixel space sampling method compared to the discrete pixel space sampling method based on pixelwise contrastive loss. The pixelwise distribution loss regresses a set of probability distribution heatmaps aiming to minimize the divergence between the predicted heatmap and the ground truth heatmap mitigating errors in correspondences. Futhermore, the pixelwise distribution loss does not need non-matching correspondences compared to the the pixelwise contrastive loss.

Based on SIMCLR inspired frameworks [31, 32], Adrian *et al.* [33] introduced similar architecture and another novel loss function called "Pixelwise NT-Xent loss" to train DON more robustly. The pixelwise nt-xent loss consumes synthetic correspondences computed from image augmentations to train DON. Adrian *et al.*'s experiments show that

the novel loss function is invariant with respect to the batch size. Additionally adopted "*PCK@k*" metric has been adopted as in preceedings [34, 35] to evaluate and benchmark DON on cluttered scenes previously not benchmarked.

Further eliminating the need for camera pose and intrinsic information along with depth information to compute correspondences in an image pair, Yen-Chen *et al.* [36] used Neural Radiance Fields (NeRF) [37] to train DON. The NeRF recreates a 3D scene from a sequence of images captured by the smartphone camera. The correspondences are extracted from the synthetically reconstructed scene to train DON.

Concerning object poses, Manuelli *et al.* [38] offer an innovative formulation of category-level objects description using semantic 3D keypoints with the manipulation specified by geometric costs and restrictions on those keypoints. The formulation naturally enables the manipulation strategy to encompass 3D keypoint recognition, optimization-based robot action planning, and grasping-based action execution. Vecerik *et al.* [39] further introduces self-supervised techniques in keypoint prediction for robot manipulability based on [40, 41, 42, 43], significantly reducing the need for human-labelled data and providing a robust detector for semantic 3D keypoints in their setup "SEK". Its main contribution comes from considering multi-view geometry as a source of elf-supervision for keypoint-based models. Furthermore, Vecerik *et al.* [39] show the applicability of SEK to robotic tasks. It further shows how we can use unlabelled data combined with SEK to counteract the effects of domain shift and its ability to generalize across samples from the same category.

Suwajanakorn *et al.* [21] propose self-supervised geometrically consistent keypoints, exploring the idea of optimizing a representation based on a sparse collection of keypoints or landmarks, but without access to keypoint annotations. The authors devise an end-to-end geometric reasoning framework to regresses a set of geometrically consistent keypoints coined as KeypointNet. The paper shows that using two unique objective loss functions, namely, a relative pose estimation loss and a multi-view consistency goal, uncovers the consistent keypoints across multiple views and object instances. Their affine translation-equivariant design may extend to previously unknown object instances and ShapeNet [44] categories. The identified keypoints on stiff 3D pose estimation surpass those from a directly supervised learning baseline.

Combining the frameworks [9, 37, 36, 38, 39] as previously described, Simeonov *et al.* [45] introduce DNN for $SE(3)$ equivariant object representations for robot manipulation. The authors use neural energy fields to manipulate an object using semantic keypoints. Simeonov *et al.* demonstrate robot tasks of picking and placing mugs having a generalized representation.

2.2 Breakdown Analysis & Comparison of Influential SOTA

In this section, the SOTA influential to this thesis is compared for its contribution, drawbacks with respective to the thesis addressed as relative drawbacks.

Contributions	Relative Drawbacks
Self-supervised Visual Descriptor Learning for Dense Correspondence[22]	
• Trained a CNN trained on contrastive loss to compute descriptors. • Produced descriptors are invariant to viewpoint & illumination.	• Using SIFT for correspondence mapping isn't spatially accurate.
Dense Object Nets: Learning Dense Visual Object Descriptors By and For Robotic Manipulation[9]	
• Used camera-based transformation to map correspondence in image pairs to train DON. • Introduced a quick trainable DNN called DON. • Formulated "Pixelwise Constrastive Loss" to train DON. • The descriptors computed from DON can generalize an object.	• The loss function is dependent on number of correspondences. • The network performance degrades while training for batch size > 1. • The descriptors have non-optimal spatial expectations when queried.
Dense Visual Learning for Robot Manipulation[30]	
• Introduced "Pixelwise Distribution Loss" robust against incorrect correspondence sampling encountered by pixelwise contrastive loss. • The pixelwise distribution loss not need non-matching correspondence to train DON.	• The pixelwise distributional loss function cannot accomodate same objects in an image while training.

Continued on next page

Breakdown Analysis & Comparison of Influential SOTA – continued

Contributions	Relative Drawbacks
Supervised Training of Dense Object Nets using Optimal Descriptors for Industrial Robotic Applications[14]	
• Emphasized that DON's are not efficient while training on small & shiny objects due to noisy correspondence generated from the consumer grade depth cameras. • Used 3D model with Laplacian Eigenmaps for supervised training of DON.	• Used 3D models to remap objects in images for reconstructing depths. • Laplacian Eigenmaps are computational costly and do not handle occlusion.
Fully Self-Supervised Class Awareness in Dense Object Descriptors[29]	
• Introduced loss functions to train DON in an unsupervised manner. • The loss functions introduced hard and soft margins to pixelwise contrastive loss.	• Does not handle occluded scenes.
Efficient and Robust Training of Dense Object Nets for Multi-Object Robot Manipulation[33]	
• Adapted NTXent-Loss on a pixelwise scale to train multiobject scene DON. • Proposed that DON relies on color hues of objects to reconstruct geometric priors. • Benchmarked all DON loss functions. • Used synthetic correspondences to train DON without depth information.	• Did not accomodate training DON that belongs to the same class.

Continued on next page

Breakdown Analysis & Comparison of Influential SOTA – continued

Contributions	Relative Drawbacks
NeRF-Supervision: Learning Dense Object Descriptors from Neural Radiance Fields[36]	
• Used NeRF to train DON making it robust against shiny surfaces.	• NeRF does not work in multi-object scences where an object is missing in another viewpoint.
kPAM: Keypoint Affordances for Category-Level Robotic Manipulation[38]	
• Introduced object representation using 3D-Keypoints to generalize pose. • Avoids task-inappropriate geometric information.	
S3K: Self-Supervised Semantic Keypoints for Robotic Manipulation via Multi-View Consistency[39]	
• Improved object representation with semantic 3D-keypoints. • Used multi-view consistency loss for training robustly against occlusion, noise and absence of visible texture.	
Discovery of Latent 3D Keypoints via End-to-end Geometric Reasoning[21]	
• Introduced 'KeypointNet' for geometric reasoning. • Used pretrained orientation network for making predictions on symmetrical objects more robust. • Used self-supervised loss functions with end-to-end training methods.	• Uses chordal distances for computing distances in rotational matrices. • Accomodates objects belonging to the same class.

Continued on next page

Breakdown Analysis & Comparison of Influential SOTA – continued

Contributions	**Relative Drawbacks**
Neural Descriptor Fields: SE(3)-Equivariant Object Representations for Manipulation[45]	
• Used neural descriptor model to fuse models of DON, Kpam[38] and NeRF for object manipulation. • Used neural energy fields to find generalized keypoints for manipulation. • Used self-supervised loss functions with end-to-end training methods.	• Need robot demonstrations to train the neural networks.

Table 2.1: Comparison of influential SOTA.

3 Objective

This thesis focuses on engineering a single semantic class-generalized label ($x \in \mathbb{R}^D$) acting as a robot grasping point in an image. If no possible labels are found in the image search space, then KeypointNet is deployed as a fail-safe to regress geometrically consistent keypoints on the object in turn generating a valid 6D-Pose of the object for robot grasping.

As the recent rasearch preceedings [9, 33, 10, 11] introduced different CNN-based Residual Network (ResNet) [46] architectures and loss functions to implement DON, the best combination of ResNet architecture and loss function will be chosen by benchmarking all the valid combinations.

Furthermore, one object will be selected for generalization using DON to manually store a valid specific generealized label for robot grasping. To eliminate the process of manually selecting labels, KeypointNet will be implemented.

Based on the availability of the datasets, synthetic data [47] will be generated to train the neural networks if no ready datasets are available.

4 Methodology

4.1 Dense Object Nets

DON is a recently proposed self-supervised contrastive DNN framework. The framework's network architecture is based on adaptation of SimCLR[48] architecture. While the SimCLR architecture encodes the entire image to an embedding of dimension using the contrastive loss function as described in Equation 4.1, the DON, encodes each pixel in an image to embedding space called dense object descriptors as described in Equation 4.2. The image with dense object descriptors as pixels is referred as dense descriptor image.

Figure 4.1: DON architecture.

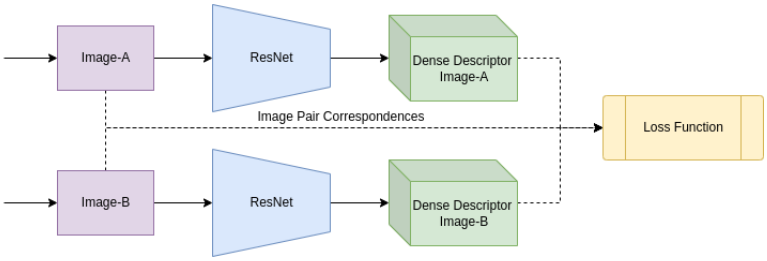

$$f_{SimCLR} : I \in \mathbb{R}^{H \times W \times 3} \rightarrow x \in \mathbb{R}^{D} \quad \text{, s.t. } D \in \mathbb{N}^{+}. \tag{4.1}$$

$$f_{DON} : I \in \mathbb{R}^{H \times W \times 3} \rightarrow I_D \in \mathbb{R}^{H \times W \times D} \quad \text{, s.t. } D \in \mathbb{N}^{+}. \tag{4.2}$$

Furthermore, according to Adrian *et al.* [33], DON relies on sequence of images in the dataset to embed each pixel to descriptor space by exploiting the geometric prior of objects based on color-hues inturn, generalizing the object.

The ResNet is usually optimized using mutual image correspondence information of image pairs with contrastive learning on a pixel scale. The trained network computes a embeddings such that (s.t.) the pixel has an unique embedding compared to the rest of the pixels. The network's visual embedding is invariant to a viewpoint and illumination and comes with the inherent property of generalizing same-class objects. The visual embedding uniquely describes the pixel locally in an image; hence, referred to as a local descriptor. The contribution of DON is thus its immense ability to generalize for other similar objects within a class without a need to train the network for each such object.

4.1.1 Implementation Strategy

Introduced in 2019, DON is young in the research field and applied for use cases in 2021. In earlier years, the authors of DON proposed "Pixelwise Distribution Loss" to improve "Pixelwise Contrastive loss". This year, researchers Adrian *et al.* [33] introduced a new loss function called "Pixelwise NT-Xent Loss" to make DON robust. The implemented use cases [10, 11, 12] used different ResNet architecture variants giving an opportunity to test combinations of loss functions with architectures to optimize the network.

4.1.2 ResNet Architectures

ResNet-N means that the DNN has N convolution layers with shortcuts between them aiding better optimization [46]. E.g., ResNet-34 consists of 34 weighted layers. Originally proposed, ResNet-34 came with few design rules; to maintain the temporal complexity per layer, the layers had the same number of filters for the same output feature map size, and the number of filters doubled in that scenario. The identity shortcuts were employed directly as the input and output dimensions stand the same.

With an increase in dimensions, there were two options to consider. The initial assumption was that the shortcut would continue to conduct identity mapping while padding extra zero entries for expanding dimensions. The other option was to utilize the projection shortcut to match dimensions.

The ResNet-50 inherits architecture from the ResNet-34 model, with revision in the bottleneck design. Each of the ResNet-34's 2-layer blocks was replaced with a 3-layer bottleneck block, resulting in the deeper ResNet-50 design.

4.1.3 Loss Functions

Pixelwise Contrastive Loss

The pixelwise constrastive loss is adapted from [48] on a pixelwise scale. The pixelwise contrastive loss brought in the concept of DON itself introduced by Florence *et al.* [9]. The pixelwise constrastive loss function aims to minimize the distance between the embeddings corresponding to a match, while the embeddings corresponding to a non-match are set at least by a marginal distance M apart. The loss function is described as,

$$\mathcal{L}_{matches} = \frac{1}{N_{matches}} \sum_{i,j}^{N} \left\| f(I_a)[x_i, y_j] - f(I_b)[x_i, y_j] \right\|, \tag{4.3}$$

$$\mathcal{L}_{non-matches} = \frac{1}{N_{non-matches}} \sum_{i,j}^{N} max(0,\ M - \left\| f(I_a)[x_i, y_j] - f(I_b)[x_i, y_j] \right\|), \tag{4.4}$$

$$\mathcal{L}_{Total} = \mathcal{L}_{matches} + \mathcal{L}_{non-matches}. \tag{4.5}$$

M is a hyperparameter and has to be chosen optimally while training the network. The loss function is sensitive to batch size and number of correspondences [33, 30]. Additionally, non-matching correspondences needs to be sampled for training the network. This thesis is not going to benchmark this loss function as it is outdated and comes with drawbacks compared to newly proposed loss functions.

Pixelwise Distribution Loss

Introduced in Florence *et al.* [9], the pixelwise distribution loss function aims to compute a set of probability distributions for each keypoint $k = \{1, 2, \dots K\}$ minimizing the divergence between the predicted heatmap and the ground truth heatmap described as,

$$p_a(x_i, y_i | f(I_a), f(I_b), x_b, y_b) = \frac{K(f(I_b)[x_b, y_b], f(I_a)[x_i, y_j])}{\sum_{i',j'} K(f(I_b)[x_b, y_b], f(I_a)[x'_i, y'_j])}, \tag{4.6}$$

where, the $K : (\mathbb{R}^{\mathbb{N}^+}, \mathbb{R}^{\mathbb{N}^+}) \to \mathbb{R}$ is a kernel function and it can be of any formulation as long as it yields a scalar ($\mathbb{R}$) processing two vectors of the same dimension. The term, $p_a(x_i, y_i | f(I_a), f(I_b), x_b, y_b) \in [0, 1]$ is the spatial probability of a keypoint in $f(I_a)[x_a, y_a]$ in the image $f(I_b)$.

The spatial expectation from the spatial probability is computed as,

$$\hat{x_b} = \sum_{i}^{W} p_a(x_i | f(I_a), f(I_b), x_b) x_i, \tag{4.7}$$

$$\hat{y_b} = \sum_{i}^{H} p_a(y_i | f(I_a), f(I_b), y_b) y_i, \tag{4.8}$$

The spatial loss of $I_a[x_a, y_a]$ in $I_b[x_b, y_b]$ is computed as,

$$\mathcal{L}_{b \to a} = \|x_b - \hat{x_b}\| + \|y_b - \hat{y_b}\|, \tag{4.9}$$

The total bi-directional loss is computed as,

$$\mathcal{L}_{Total} = \mathcal{L}_{b \to a} + \mathcal{L}_{a \to b}, \tag{4.10}$$

The kernel functional chosen to compute the bi-directional loss function,

$$K : (f(I_a)[x_i, y_i], f(I_b)[x_b, y_b]) \to exp(-\|f(I_a)[x_i, y_i] - f(I_b)[x_b, y_b]\|). \tag{4.11}$$

This pixelwise distribution loss function can be implemented in a batch fashion yielding high-performance computation time in a computer. Furthermore, The Figure 4.2

Figure 4.2: 2D spatial expectation of keypoint in two images.
Source: [30]

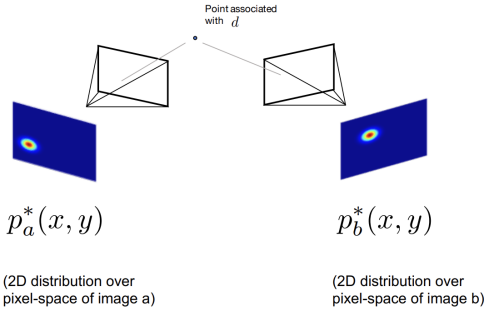

intuitively illustrates the spatial expectation of a keypoint in two images.

Furthermore, the loss function improves spatial expectation of a descriptor compared to the pixelwise contrastive loss, yielding better results in the search space of a descriptor in a new image. One of the drawbacks of using this loss function is that only one object belonging to the same class in an image can be used while training the neural network. Having more objects belonging to the same class yields faulty prediction of spatial expectations.

Pixelwise NT-Xent Loss

The "NT-Xent loss" is originally introduced in Chen *et al.* [48] adopted by Oord *et al.* [49] to encode an entire image to an embedding and implemented on a pixel level to train DON by Adrian *et al.* [33]. The authors Adrian *et al.* [33] randomly sample N correspondences from an image pair (I_A, I_B), with each correspondence yielding two descriptors d_i^A and d_i^B , for a total of N pairs, or $2N$ descriptors. For a given descriptor, all other $2(N-1)$ descriptors are respectively treated as negative examples. The below given loss function is directly optimized against the descriptor pair,

$$\mathcal{L}_{i,j} = -\log \frac{\exp(K(d_i, d_j)/\tau)}{\sum_{k=1,k\neq i}^{2N} \exp(K(d_i, d_j)/\tau)}, \tag{4.12}$$

where, $\tau \in \mathbb{R}^+$ is a temperature scaling factor and K is cosine similarity kernel defined as,

$$K = \frac{\langle d_i, d_j \rangle}{\|d_i\| \|d_j\|} \quad \text{, s.t. } d_{i,j} \in \mathbb{R}^{\mathbb{N}^+},\ K \in [1, 0]. \tag{4.13}$$

Since K takes only positive inputs, unlike the cosine function, it produces the outputs in the range $[0, 1]$ which leads to its interpretation as in expression refer equation 4.14.

$$K(d_i, d_j) = \begin{cases} 1 & \implies (d_i, d_j) \text{ are similar.} \\ 0 & \implies (d_i, d_j) \text{ are dissimilar.} \end{cases} \tag{4.14}$$

One of the drawbacks of the pixelwise nt-xent loss function is that semantically closer objects in an image are treated as two different objects which in turn hinders the generalizing properties of the neural networks.

4.1.4 *PCK@k* as an Evaluation Metric

To measure the performance of the network, "*PCK@k*" evaluation metric is adopted as in preceding works [50, 33]. *PCK@k* is defined for a set of pixel pairs $\mathcal{T} = \{p_i, q_i\}_{i=1}^{N}$ as follows,

$$PCK@k(\mathcal{T}) = \frac{1}{|\mathcal{T}|} \sum_{(p_i,q_i)\in\mathcal{T}} [\|p_i - q_i\| \leq k] \quad \text{, s.t. } (p_i, q_i) \in \mathbb{R}^{\mathbb{N}^+}, (k, \mathcal{T}) \in \mathbb{R}, \tag{4.15}$$

where k is the maximum error allowed in turn, influencing the Iverson bracket $[\,\cdot\,]$ to 1 if the error is within the limits of k and 0 otherwise. $\mathcal{T}$ is a number of keypoints (p_i, q_i) normalizing the computed metric. Instead of using L^2-Norm to compute the error between keypoints, it is replaced by a kernel function 'D' similarly in equation 4.13 in page 16 bringing in more flexibility. The kernel revised metric is described as,

$$PCK@k(\mathcal{T}) = \frac{1}{|\mathcal{T}|} \sum_{(p_i,q_i)\in\mathcal{T}} D(p_i, q_i) \leq k. \tag{4.16}$$

4.1.5 Suzanne, a synthetic dataset

To train and benchmark DON, no compatible ready datasets are available. The datasets available either missed camera information like intrinsics or extrinsics parameters, masks information or captured same objects belonging to the same class in an image, posing ill-conditions to benchmark pixelwise distribution loss.

To overcome this situtation, 'BlenderProc' [51] is used to generate synthetic dataset with all annotations needed to train DON. 'Suzanne' is a model already available in the render tool and is placed in the world datum center. For this control dataset, 100 random cameras are added in the environment with random poses capturing depth, extrinsic information and mask for each viewpoint. The Table 4.1 in page 18, provides the preview of dataset. The annotated pixels in blue in second image from right to left in Table 4.1 projects the correspondences through world coordinates in the first image from right to left annotated in red. As the dataset produces perfect depth maps of the objects in the images, the benchmarking metrics might not tally with available benchmarked results.

Dataset Preview			
RGB	Depth	Mask	Correspondences Mapping
	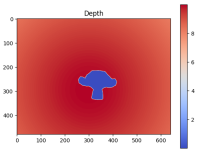		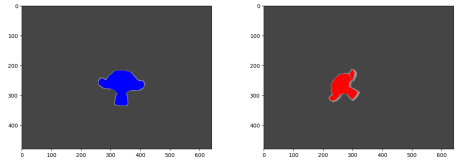

Table 4.1: Depiction of dataset quintennsials features of dataset

Following the procedure in [28], the correspondences are computed in an image pair described as follows:
The camera extrinsic parameters ($\mathcal{T}_{C\to W} \in \mathbb{R}^{4\times4}$) is the camera pose relative to the world frame. The camera intrinsics is defined as $\mathcal{I} \in \mathbb{R}^{3\times3}$. To map the correspondences from image I_a to image I_b, the pixels from the image $[u, v]^T \in I_a \in \mathbb{R}^{2\times1}$ are projected to the world coordinates $W_a \in \mathbb{R}^{3\times1}$ using depth (d) and from the world coordinates to the image I_b as follows:

$$W_a = \mathcal{T}^a_{C\to W}\, \mathcal{I}^{-a} \begin{bmatrix} u^a \\ v^a \end{bmatrix} d^a_{uv} \tag{4.17}$$

The computed world coordinates from I_a, W_a are projected to pixels in I_b,

$$d^b_{uv} \begin{bmatrix} u^b \\ v^b \end{bmatrix} = \mathcal{I}^b\, \mathcal{T}^{-b}_{C\to W}\, W_a, \tag{4.18}$$

where,

$$\mathcal{T}^{-b}_{C\to W} = \begin{bmatrix} R^b & -R^b t^b \\ 0^T_3 & 1 \end{bmatrix}, \quad \text{s.t. } R^b \in SO(3). \tag{4.19}$$

Additionally, mask is used to sample the pixels from I_a within the object silhouette.

4.1.6 Manual Method for Robot Grasp Generation

The DON produces visual embeddings ($f(I)[u, v] \to d, \quad d \in \mathbb{R}^{\mathbb{N}+}$) such that each pixels withholds unique embedding in descriptor space reducing computational complexity to find the same pixel in different viewpoint in an RGB space omitting complex search algorithm. Using "Pygame" [52] library in python, an interactive application is developed to pick descriptors in the descriptor space with it's image coordinates $[u, v]^T$ using depth and camera intrinsics to project them to the coordinates in the camera frame. More than three descriptors are picked such that it produces a valid rotation matrix via PCA or SVD and the mean value acting as a center to generate a 6D pose defined as,

$$\mathcal{T} = \begin{bmatrix} R & t \\ 0^T_3 & 1 \end{bmatrix} \in \mathbb{R}^{4\times4}, \quad \text{s.t. } R \in SO(3),\ t \in \mathbb{R}^{3\times1}, \tag{4.20}$$

The interactive application allows to save multiple object pose definition file and this definition file is loaded into an other application to search and compute multiple object 6D pose information in an other or same image. The descriptors are searched using gaussian kernel derived from heat kernel formulation,

$$\mathbb{E}[u^*, v^*]_d = \underset{u_i, v_i}{\operatorname{argmin}}\ exp - \left(\frac{\| (f(I_a)[u_i, v_i] - d) \|}{exp(t)} \right)^2 \tag{4.21}$$

Where $t \in \mathbb{R}$ controls the kernel width influencing the search space to compute the spatial expectation of the query descriptor d in image I_a. The descriptors produced by DON are supposedly to be robust against color jitters, illumination changes and occlusions in order to produce consistent 6D poses [33].

To compute the relative 6D pose of an object in the new viewpoint of the camera, the queried keypoint locations are redordered in the matrix respective to the keypoint and its spatial locations as stored in the definition file. If a keypoint is not found, then the keypoint in the definition file is omitted and mutually rearranged. The queried keypoint locations produce relative 6D pose $\mathcal{T}_{object}$ compared to the pose stored in the definition file as,

$$\mathcal{T}_{rel} = (\mathcal{T}_{def}^T \, \mathcal{T}_{def})^{-1} \, \mathcal{T}_{def}^T \, \mathcal{T}_{object}. \tag{4.22}$$

To eliminate the manual process of annotating keypoints to genetate robot grasps, KeypoinNet is implemented.

4.2 KeypointNet

KeypointNet is a framework for end-to-end geometric reasoning that regresses the best set of category-specific 3D keypoints with their associated detectors, i.e., higher-dimensional generalized embeddings. By definition, KeypointNet works for an image pair. This framework estimates 3D pose by giving a differentiable goal that seeks the optimal set of keypoints to recover the relative pose of an item between two viewpoints. Hence, KeypointNet allows for predicting geometrically and semantically consistent keypoints across viewing angles and instances of an object category by optimizing four loss functions.

4.2.1 Loss functions

The KeypointNet produces N number of spatial probabilities for N keypoints described by $g_i(u, v) \in \mathbb{R}^{W \times H}$, s.t. $\sum_{u,v} g(u, v) = 1$. The pixel spatial expectations is computed via continuous sampling method described by,

$$[u_i, v_i]^T = \left[\sum_{u,v} g_i(u,v) * u, \sum_{u,v} g_i(u,v) * v \right]^T, \quad \text{s.t. } g_i(u,v) \in \mathbb{R}^{W \times H}. \tag{4.23}$$

Similarly, depth is computed as follows:

$$d_i = \sum_{u,v} g_i(u,v) * d_i[u,v], \quad \text{s.t. } d_i(u,v) \in \mathbb{R}^{W \times H}. \tag{4.24}$$

The self-supervised training of this network is based on the following loss functions.

Multiview Consistency Loss

The multiview consistency loss function enforces the network to regress keypoint expectations at same the locations in an image pair. Concisely, a keypoint in one image should project on a pixel location corresponding to a keypoint in another image. To achieve this, pixels are projected to the camera frame using depth and intrinsic information. Using mutual transformation information between two cameras, the pixels are further projected back to the pixel frame of the second camera. The loss is then the distance between the projected pixel location and regressed keypoint's pixel location.

To make this formulation more intuitive, the originally proposed method is altered. Instead, of evaluating the keypoints in pixel frame, they are evaluated in the world frame. The idealogy is that the object is fixed in the world datum and camera poses changes preserving the object coordinates in the world frame as depicted in Figure 4.2 in page 16. The altered multiview consistency loss function is defined as,

$$\mathcal{L}_{mvc} = \frac{1}{N} \sum_{i=1}^{N} \| W_A^i - W_B^i \|, \quad \text{s.t. } W_{A,B} \in \mathbb{R}^{3 \times 1}. \tag{4.25}$$

Relative Pose Loss

As the KeypoinNet produces N number of keypoints, the keypoint locations together projected into the camera frame coordinates produces a 6D pose computed. The relative pose loss function rearranges the keypoint locations in an image preserving the object's 6D pose in the viewpoint respective to the camera pose. Additionally, this preserves the relative pose between two camera poses and relative pose generated from the keypoint locations in an image pair.

As per the original implementation of the KeypointNet, the authors discard the relative translation and expressed the relative pose loss in form of chordal distance between two rotational matrices $\in SO(3)$ using Frobenius-Norm [53] as:

$$\mathcal{L}_{pose} = 2 \arcsin \left(\frac{1}{2\sqrt{2}} \left\| \hat{R} - R \right\|_F \right) \quad \text{, s.t. } R \in SO(3). \tag{4.26}$$

Where, $\hat{R}$ is the groundtruth relative rotation of camera-a pose in the world frame and camera-b pose in the world frame and R is the predicted relative rotation of regressed keypoints in an image pair. The Frobenius norm yields the chordal distance in range $[0, 2\sqrt{2}]$ which is normalized in the implementation. The chordal distance formulation satisfying the triangle inequality condition involves "*some messy algebra*" [54] as the operation $\hat{R} - R \notin SO(3)$.

To make this more geometrically intuitive, the poses $\in SE(3)$ are transported to *Riemannian manifold* [55]. *Riemannian manifold* is rich in geometry and differentiably smooth. Instead, of expressing the distance in chordal form, 'geodesic-distance' is chosen as it is smooth on for infinitesimally small trajectories on the manifold. Here, the trajectory is defined as the distance to be covered such that the two rotation matrices align with each other.

The manifold geometry consists of two parts, i.e., a manifold and a tangential plane tangential place $T(\mathcal{M}^p)$ represented as a tangential Euclidean space to the manifold, and the manifold space. the manifold space $\mathcal{M}^p : p \in \mathbb{R}^{N^+}$. Exp-maps and log-maps refer equation 4.28 are used to transport a vector on tangential plane to the manifold and vice versa.

$$expmap : \mathfrak{so}(3) \rightarrow SO(3), \tag{4.27}$$

$$logmap : SO(3) \rightarrow \mathfrak{so}(3). \tag{4.28}$$

Here $r(\alpha) \in \mathfrak{so}(3) \in T(\mathcal{M}^p)$ is a skew-symmetric matrix built from the axis angles $\alpha \in \mathbb{R}^3$ described as,

$$r(\alpha) = \begin{bmatrix} 0 & -z & y \\ z & 0 & -x \\ -y & x & 0 \end{bmatrix} \quad \text{, s.t. } \alpha = [x, y, z]^T \in \mathbb{R}^3. \tag{4.29}$$

The object or camera's rotation in the dataset is represented as $SO(3)$.

The geodesic distance is a *bi-invariant* metric on $SO(3)$ with range$[0, \pi]$:

$$\mathcal{L}_{pose} = \frac{1}{\sqrt{2}} \| logmap(\hat{R}^T R) \|_F = \frac{1}{2} \| logmap(\hat{R}^T R) \|. \tag{4.30}$$

The $\mathcal{L}_{pose}$ is substituted in the place of original loss function formulation. The relative groundtruth rotation $(\hat{R})$ for the loss is computed as:

$$\hat{R} = \hat{R}_{A \rightarrow B} = \hat{R}_A^T \, \hat{R}_B \quad \text{, s.t. } \hat{R} \in SO(3). \tag{4.31}$$

where, $\hat{R} = \hat{R}_{A \rightarrow B} \in \mathbb{R}^{3 \times 3}$ is the groundtruth relative rotation of camera-a pose in world $\hat{R}_A$ and camera-b pose in the world $\hat{R}_B$. The camera poses are the extrinsic matrices

available in the dataset. To compute the relative rotation R of regressed keypoints in an image pair, i.e., $X_A, X_B \in \mathbb{R}^{N\times 3}$ Kabsch's algorithm [56] is employed as follows:

$$\mathcal{H} = (X_A - X_A^{mean})^T (X_B - X_B^{mean}) \quad \text{, s.t. } \mathcal{H} \in \mathbb{R}^{3\times 3},\ X_{A,B}^{mean} = \overline{X}_{A,B}. \tag{4.32}$$

where, $\mathcal{H}$ is the covariance matrix of the mean centered keypoint locations in the camera frame. To center the keypoint locations in the camera frame, $X^{mean} \in \mathbb{R}^{1\times 3}$ is computed along the dimension N and each row in X is subtracted with the mean. The predicted relative rotation of keypoint locations in the image pair is computed as,

$$R_B = V \begin{bmatrix} 1 & 0 & 0 \\ 0 & 1 & 0 \\ 0 & 0 & det(VU^T) \end{bmatrix} U^T, \tag{4.33}$$

where,

$$U\Sigma V^T = SVD(\mathcal{H}). \tag{4.34}$$

The term $det(VU^T)$ handles the reflection case while estimating the rotation matrix. In other terms it makes the z rotation vector orthonormal to 'xy' rotation vectors such that it always points to the camera in the camera relative frame. This method to condition z rotation vector produces gradients which allows neural networks to be trained via backpropogation compared to using cross-product of vectors which does not produce gradients since the vector in the matrix is changed via inplace operation.

Separation Loss

Separation loss function penalizes cases where the distance between two keypoint locations is less than a specified margin (δ).

$$\mathcal{L}_{sep} = \frac{1}{N} \sum_{i}^{N} \sum_{j\neq i}^{N} max(0, \delta^2 - \|X_i - X_j\|^2). \tag{4.35}$$

Silhoutte Loss

Silhoutte loss functions encourages the spatial probabilities of keypoints $g_i(u, v)$ to lie with the object silhoutte:

$$\mathcal{L}_{obj} = \frac{1}{N} \sum_{i=1}^{N} -log \sum_{u,v} b[u, v]\ g_i(u, v). \tag{4.36}$$

While training the network, the mask of the object is accessible. The mask values are sampled from the pixel locations $b[u, v] \in \{0, 1\}$. The mask information is only used while training the network and is not using during the inference. If all the keypoints are regressed within the object silhoutte, the loss computes to zero.

Variance Loss

Variance loss function penalizes the spatial probabilities if they are broad in turn, encouraging peaky distribution. The broader spatial probabilities brings in more uncertainty in the keypoint spatial expectation. In turn, the loss function penalizes the uncertainty of the keypoint spatial expectation by shrinking the span of the spatial probabilities as depicted in Figure 4.3 in page 23. Furthermore, in the Figure 4.3 in page 23, the x marks the keypoint spatial expectation. The left image illustrates the broader spatial probability of a keypoint bringing in more uncertainty in the keypoint spatial location (expectation). The right image describes the peaky spatial probability of the keypoint encouraged by the loss function.

The variance loss functions is described as,

$$\mathcal{L}_{var} = \frac{1}{N}\sum_{i=1}^{N}\sum_{u,v} g_i(u,v)\left\|\mathcal{G} - [u_i, v_i]^T\right\|^2, \tag{4.37}$$

where $\mathcal{G}$ is the spatial grid of row and column indices described as,

$$\mathcal{G}_{0ij} = \begin{bmatrix} 0 & \dots & 0 \\ \vdots & \ddots & \vdots \\ H & \dots & H \end{bmatrix}, \quad \mathcal{G}_{1ij} = \begin{bmatrix} 0 & \dots & W \\ \vdots & \ddots & \vdots \\ 0 & \dots & W \end{bmatrix} \quad \text{, s.t. } \mathcal{G} \in \mathbb{R}^{2\times W\times H}. \tag{4.38}$$

Figure 4.3: Variance loss function at work.

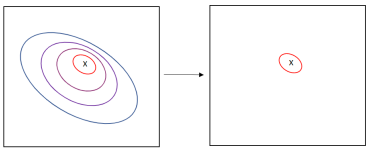

4.2.2 Total Weighted-Sum Loss

To train the network, all loss functions are weighed by their own specific weights in-turn, signifying that one loss functions needs more priority than other loss functions. The priority depends on the network architecture being used. Let's say if the multi-view consistency loss is not converging, then the weights assigned to that particular loss function are increased such that the multiview loss is further optimized by the network in the training phase. The total weighted loss function is the scalar product of the weights $W = [w_{mvc}, w_{pose}, w_{sep}, w_{obj}, w_{var}]^T$ and the individual loss functions $\mathcal{L} = [\mathcal{L}_{mvc}, \mathcal{L}_{pose}, \mathcal{L}_{sep}, \mathcal{L}_{obj}, \mathcal{L}_{var}]^T$ described as,

$$\mathcal{L}_{Total} =< W, L > \quad \text{, s.t. } \mathcal{L}_{Total} \in \mathbb{R} \;\&\; W, L \in \mathbb{R}^4. \tag{4.39}$$

Here W is a hyperparameter. The hyperparameter in this thesis implementation will be fixed by a trial-and-error process as other sampling or optimization process consumes a lot of time.

4.2.3 Network Modification

The ResNet architecture will be used over originally proposed image segmentation based CNN while preserving the part of architecture with predicting depth and spatial probabilities of the keypoints to preserve the neural network architecture homogenity with DON architecture.

Additionally, no pretrained orientation network is used to aid the KeypointNet breaking the symmetry of the objects as in [21]. As per the proposed data augmentation in [21], the data will not be scaled to a unit dimension preserving realistic conditions of object in an environment for which the network will be trained for.

4.3 End-to-End Network Training

End-to-end network training is a deep learning technique in which all parameters are taught concurrently rather than step by step. An deep learning method is trained in an end-to-end manner when a DNN needs to perform multiple tasks. Furthermore, sometimes a deep learning network learns joint features pertaining multiple tasks. Particularly in this thesis, joint features for DON representations and generalized object 6D poses are computed via generalized geometrically consistent keypoints.

4.3.1 KeypointNet Informed Dense Object Nets

The depth values produced for small & shiny objects by the consumer grade depth cameras are not accurate [14], in turn leading to inconsistent correspondences mapping between two image pairs which further leads to inaccurate training of DON. To overcome this, KeypointNet is employed as KeypointNet does not depend on the depth values of objects for training.

As per the definition, KeypointNet can be modified to generate correspondences between image pair belonging to the same class without the need of additional DNN like Universal Correspondence Network [57]. KeypointNet eliminates the need for projecting pixels from one image to another image through the world coordinates Equation 4.17 in page 18 to compute correspondences in an image pair.

Furthermore, the KeypointNet architecture is stacked on top of DON architecture such that semantic correspondences are supplied for DON seamlessly keeping it self-

supervised. Both the networks are optimized with the joint losses and not individually as described below:

$$\mathcal{L}_{Joint} = \mathcal{L}_{KeypointNet} + \mathcal{L}_{DON} \tag{4.40}$$

The joint losses produces mutual gradients for optimization such that the networks compute features which are beneficial to each other forming a coordination to fulfil a task [58].

Furthermore, DON training is delayed by few epochs and the KeypointNet is trained at the start such that the training converges faster.

4.3.2 Dense Object Nets Informed KeypointNet

Preserving the goal of the thesis, single class generalized labels need to be stored for deployment and to achieve this, DON is stacked on top of KeypointNet. As DON produces class generalized descriptors (labels) the KeypointNet is employed to pick the labels autonomously.

The KeypointNet regresses N number of keypoints in the descriptor image and each keypoint is a pixel location for the label in the descriptor image. For an object, class generalized keypoints are stored in N random probabilities. This insures that in cases of object occlusion in viewpoint, if one label is not found, another label can be recalled creating a grasping point for the robot as a counter-measure.

For better optimization, the DON is trained first and few epochs later KeypointNet is optimized better. Additionally, the joint losses is adopted as in Equation 4.40 in page 25 for optimization purposes.

4.3.3 Mining Dense Object Nets Representations in KeypointNet

The KeypointNet predicts semantic object keypoints, in turn equipping inert property for object generalization. DON computes dense generealized visual embeddings by exploiting the geometric prior of a sequence of registered RGBD frames to sample pixel correspondences between alternative views of the same object based on color hues [33].

The KeypointNet shares the same ResNet architecture as DON ushering an idea that the KeypointNet might be encompassing generalized visual embeddings similarly computed by DON. Intuitively, upsampled dense ouput features as depicted in the Figure 4.4 from the ResNet architecture in the KeypointNet might have the dense object representations.

The KeypointNet is trained with the upsampled dense feature having output channel dimension of 256 and for benchmarking purposes, it is set to $D = 16$ such that it can be

mutually benchmarked against DON computed representations.

The key adavantage here is that the dense object representations can be directly extracted by upsampling the output of the last layer without the need of training DON saving time and resources. The same procedure is employed to store prioritized labels as in section 4.3.2 in page 25.

Figure 4.4: KeypointNet Architecture.

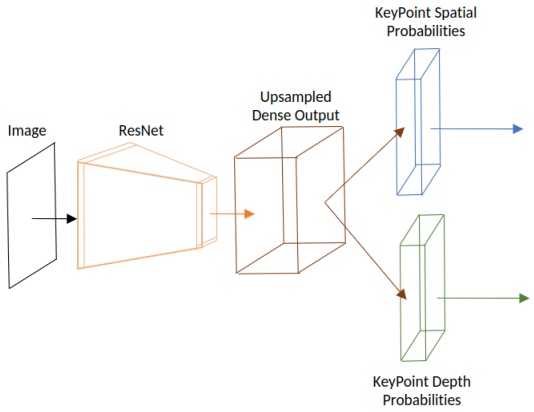

4.4 Generalizing "Caps"

The thesis moreover chooses to generalize caps. We have chosen the cap object for the further examination since the cap mesh models are readily available in the Shapenet library [44] and it was also possible to obtain the real-world cap data. Blenderproc [51] is used to generate the synthetic cap dataset similar to Suzanne dataset. Caps are chosen such that each of them have distinct shapes, designs and colors. The cap models are chosen from the Shapenet library [44] library as it possess rich object information including textures, as one can see in Table 4.2 in page 26.

Cap Dataset Preview
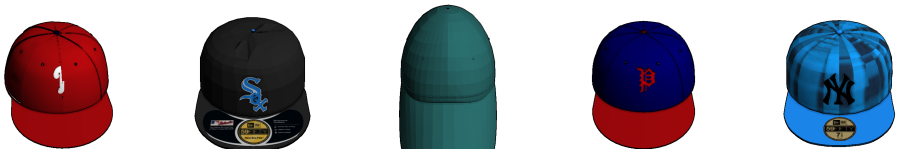

Table 4.2: Illustration of caps sampled from the Shapenet library [44].

To make the training more robust such that networks are more object-centric, the images are additionally augmented with random backgrounds and noisy backgrounds in addition to color jitter and greyscaling augmentations, as depicted in Figure 4.5 in page 27. The mask information in the synthetic dataset is used to augment the backgrounds.

Figure 4.5: The image in the right illustrates the noisy backgrounds and the image in left describes random background augmentation.

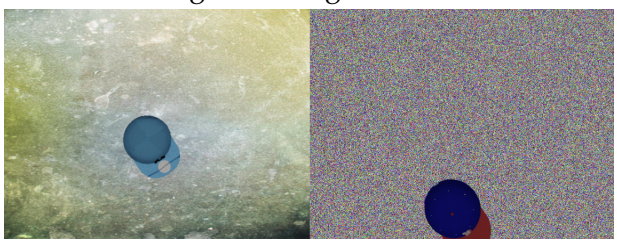

4.4.1 Semantic Correspondences Mapping Pipeline

By definition, KeypointNet regresses semantic keypoints on the objects. Meaning, the keypoint in one object is positioned semantically equivalent in an another object of the same class.

Furthermore, this property of KeypointNet of producing semantic keypoints in the inference stage and not training phase can be used as correspondences in an image pairs to train DON. Loading semantic equivalent correspondences might affect the evalutaion of DON based on *PCK@k* metric.

4.4.2 Tweaking the Training Pipeline

Loading semantic correspondences to train DON calls for a revision in the existing training pipeline. At first, the KeypointNet is trained to compute semantic correspondences across objects belonging to the same class. The pretrained KeypointNet will be used to train DON. Finally, we shall use the pretrained DON to train the KeypointNet to sample geometrically consistent single class generalized labels for robot grasping. To the best of our knowledge, such a combination of the KeypointNet and DON is novel.

"End-to-End" method of training the networks will not be used as the KeypointNet can only be trained using same object in an image pair and not semantically equivalent object. Meanwhile, DON can be trained using the semantic correspondences in an image pair.

4.4.3 Evaluating Single Class Generalized Labels in the Wild

The expression "in the Wild" denotes the case when the sampled single class generalized labels are evaluated against images which are not in the training pipeline. The images of caps used for evaluation will be fetched from a smartphone camera.

Furhermore, the single class generalized labels for evaluation are autonomously picked from the KeypointNet trained on the DON representation.

4.4.4 Robot Grasping Pipeline

To develop the robot grasping pipeline, Franka Emika 7-DOF robot manipulator is used. It is one of the robots available at sereact [1] equipped with hardware to run artificial intelligence algorithms. The robot is equipped with the 2-jaw parallel gripper. Futhermore, Intel Realsense D435 camera is wrist-mounted as illustrated in Figure 4.6.

Figure 4.6: Robot setup for cap grasping with wrist-mounted camera.

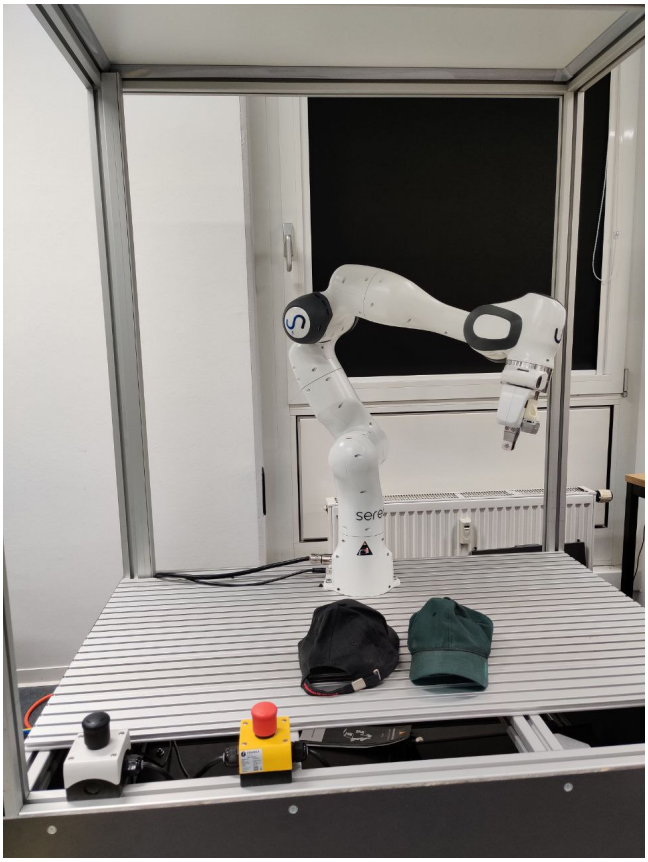

The RGB image is streamed into the neural networks to compute dense object descriptors from DON and 6D pose produced from keypoints from the KeypointNet. By using pre-computed single class generalized labels stored offline, the Guassian kernel from Equation 4.21 in page 19 is employed to produce grasping points for the robot. The depth information along with camera extrinsic and intrinsic information is used to project the spatial expectation of the queried label (descriptor) to camera frame coordinate for robot grasping.

5 Results

5.1 Dense Object Nets

For benchmarking, 48GB VRAM GPU is used. As per the VRAM availability, the ResNet architecture with pixelwise distribution and pixelwise nt-xent loss are evaluated with 2048 correspondences for an image pair with the descriptor dimension $D = 3$ and batch size of 2. Additionally, both the loss functions are benchmarked with 512 correspondences for an image pair with descriptor dimension $D = 16$ and batch size of 2. Each model is trained for 100 epochs with Adam optimizer [59] initialized with learning rate of 3×10^{-5} with weight regularization of 1×10^{-4}. Minimum validation loss is monitored to save best model. Each epoch took $45s$. Training DON with the pixelwise distribution loss occupies less VRAM compared to the pixelwise nt-xent loss.

The *PCK@k* metric Equation 4.15 is computed following the procedure described in [33]. The benchmark results are presented in Table 5.1, where the numbers in bold mark the optimal benchmark result ($\uparrow$ signifies higher score is better). The optimal benchmark result is decided based minimum validation loss and computation costs.

The results have higher values compared to benchmarking results in preceeding [33] as the model is evaluated for a single object scene rather than for a multi-object scene as described in [33]. The pixelwise distribution loss outperforms the pixelwise contrastive loss for a single object scene in accordance to the benchmarks in [33].

Benchmarking DON for $AUC \pm \sigma \; for \; PCK@K \uparrow$				
Loss Functions	D	ResNet-18	ResNet-34	ResNet-50
Pixelwise Distribution	3	**0.9800**	0.9800	0.9800
Pixelwise Distribution	16	0.9800	0.9800	0.9800
Pixelwise NT-Xent	3	0.9791 ± 0.0003	0.9796 ± 0.0003	0.9798 ± 0.0001
Pixelwise NT-Xent	16	0.9799 ± 0.0005	**0.9800**	0.9776 ± 0.0039

Table 5.1: DON evaluation against $AUC \pm \sigma \; for \; PCK@K$ metric.

As for the descriptor dimension $D = 3$ the pixelwise distribution loss produces consistent results, as described in Table 5.1, it is evident that the pixelwise distribution loss produces optimal descriptors with respect to keypoint spatial expectation compared to

Visual Inspection of Descriptor Image	
Pixelwise distribution loss	Pixelwise NT-Xent loss
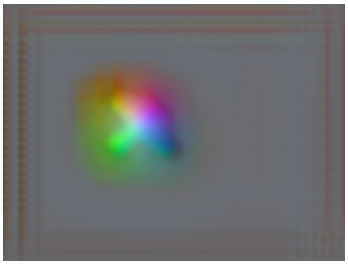	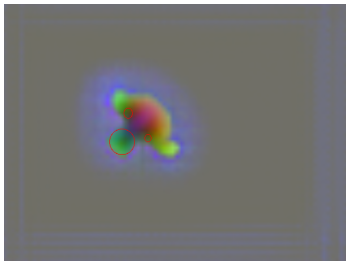

Table 5.2: Visual inspection for optimal placement of descriptors.

the pixelwise nt-xent loss and is chosen for further implementation.

To compare both the loss functions visually, the dense descriptor image is extracted from the DON and color encoded by scaling the descriptor ($d \in \mathbb{R}^3$) to the pixel space of $p \in \mathbb{R}^3$, s.t. $p \in [0, 255]$. By definition, the dense descriptors are locally unique to each other. As described in Table 5.2, the descriptors encoded by the network trained on the pixelwise nt-xent loss yields the non-optimal descriptors (annotated in red circles in the right image) compared to the network trained on pixelwise distribution loss which performs better.

5.1.1 Manual Method for Robot Grasp Generation

In the interactive application developed, the descriptors are selected manually. The manually selected descriptors pixels locations are projected to camera frame using depth and camera intrinsics to produce a 6D pose computed via PCA. The DON produces consistent descriptors against color jitter, occlusion, illumination and viewpoint detailed in Table 5.3. Furthermore, the 6D pose generated via the interactive application is not benchmarked as it is developed to test the consistency of the descriptors produced by DON addtionally, the pose produced by PCA has different basis compared to poses present in the dataset.

Illustration of Robust Descriptors		
Color Jitter	Illumination Changes	Occlusions
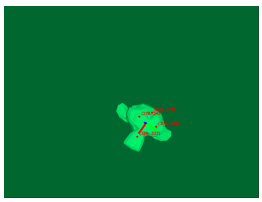	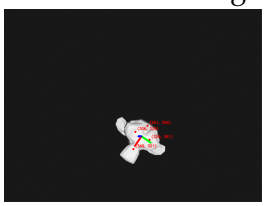	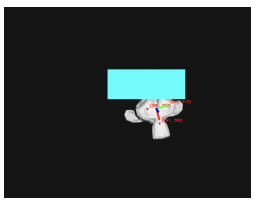

Table 5.3: Testing descriptors for robost 6D pose generation.

5.2 KeypointNet

The ResNet architecture is used to train KeypointNet task for 1000 epochs with batch size 16. To train the network, ADAM optimizer is used with the learning rate of 1×10^{-3} with no weight regularization. The optimal weights to compute to weighted sum loss in Equation 4.39 in page 23 is set to $W = [1.0, 0.2, 1.0, 1.0, 0.0001]^T$. The ResNet-18 and ResNet-34 architectures are trained to predict 8, 16, 32 number of geometrically consistent keypoints with $\delta = 10$ pixel spacing margin. The models are saved monitoring the minimum validation loss while training.

To benchmark the KeypointNet, the losses used to train the network itself is applied as it captures information like multiview consistency, relative pose, and whether a keypoint belongs to an object silhoutte, which are the pivotal properties that a keypoint must carry. The Table 5.4 describes the benchmarking results sampled from 10 random image pairs. ($\downarrow$ in the Table 5.4 represents that lower score is better.)

KeypointNet Benchmarking $\downarrow$					
Model	N	$\mathcal{L}_{mc}$	$\mathcal{L}_{pose}$	$\mathcal{L}_{obj}$	$\mathcal{L}_{sep}$
ResNet-18	8	0.1720 ± 0.0545	0.0826 ± 0.1123	0 ± 0	0 ± 0
ResNet-34	8	0.1115 ± 0.0244	0.1303 ± 0.1325	0 ± 0	0.0084 ± 0.0465
ResNet-18	16	0.2121 ± 0.0676	0.1427 ± 0.1332	0 ± 0	0.2745 ± 0.0576
ResNet-34	16	0.0830 ± 0.0891	0.0732 ± 0.0891	0.1813 ± 0.2142	0 ± 0
ResNet-18	32	1.0130 ± 0.2978	0.0990 ± 0.1276	1.3405 ± 0.3274	0.0088 ± 0.0234
ResNet-34	32	0.4206 ± 0.1906	0.0974 ± 0.0990	0.0928 ± 0.2440	0.0122 ± 0.0508
ResNet-50	32	0.1983 ± 0.6378	0.1312 ± 0.1262	1.3815 ± 0	0.2019 ± 0.0829

Table 5.4: Benchmarking KeypointNet with individual losses.

As per the benchmarking results in Table 5.4 in page 32, the ResNet-34 performs better overall. As per the ResNet-18 training history, the validation loss increases after some epochs and does not predict with consistent lower validation loss while, the ResNet-34 yields consistent decreasing in validation loss till the end of the training refer Figure 5.1. Additionally, ResNet-50 is benchmarked to predict 32 keypoints and found under performing. Hence, ResNet-34 architecture instead will be used for future implementation.

Figure 5.1: Output of trained ResNet-34 for KeypointNet task.

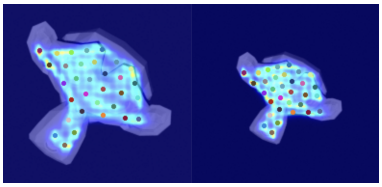

5.3 End-to-End Training

5.3.1 KeypointNet Informed Dense Object Nets

The ResNet-34 is used to implement KeypointNet tasks supplying 256 number of correspondences per image implying 512 correspondences for an image pair to train ResNet-18 based DON with margin $\delta = 3$ pixel apart. DON is trained with pixelwise distribution loss with the descriptor dimension $D = 3$. Adam optimizer is used to train the networks jointly with learning rate of 1×10^{-3} and no weight regularization. W for training the KeypointNet loss is set to the same value as used in KeypointNet benchmarking. The benchmarked results in Table 5.5 in page 33 are computed by extracting output features from the individual networks stacked to train in end-to-end training fashion.

KeypointNet Informed DON Benchmarking				
DON	$AUC \pm \sigma$ *for PCK@Kmetric*			
	0.9666 ± 0.0034			
KeypointNet	$\mathcal{L}_{mc}$	$\mathcal{L}_{pose}$	$\mathcal{L}_{obj}$	$\mathcal{L}_{sep}$
	0.4367 ± 0.9020	0.0893 ± 0.1897	0.0019 ± 0.0020	0.0957 ± 0.0160

Table 5.5: Benchmarking KeypointNet informed DON for their individual performance.

The DON performance descreases compared to the bechmarking results in Table 5.1 in page 30. The keypoints computed from the KeypointNet are not consistent as one can see for $\mathcal{L}_{mc}$ in Table 5.5. As the inconsistent keypoints are supplied to DON for training, the performance of DON decreases. Furthermore, the pixelwise distribution loss is not robust to inconsistent correspondence as claimed in [30].

5.3.2 Dense Object Nets Informed KeypointNet

The ResNet-18 is used to train DON of the descriptor dimension $D = 3$ with 256 correspondences per image implying 512 correspondences are sampled to train an image pair. The ResNet-34 is used to train KeypointNet predicting 8 keypoints on dense object representations with $\delta = 10$ pixels apart to pick lables. ADAM optimizer is used to train the networks jointly with learning rate of 1×10^{-3} and no weight regularization. W for training the KeypointNet loss is set to the same value as used in KeypointNet benchmarking. The benchmarked results in Table 5.6 in page 34 are computed by extracting output features from the individual networks stacked to train in end-to-end training fashion.

As per the benchmarking results in Table 5.6, the performance of DON decreases as the number of correspondences to train the DON network is limited to 256 for an image. This implies that all the loss functions to train the DON are sensitive to number of correspondences.

DON Informed KeypointNet Benchmarking				
DON	$AUC \pm \sigma \; for \; PCK@Kmetric$			
	0.9756 ± 0.0005			
KeypointNet	$\mathcal{L}_{mc}$	$\mathcal{L}_{pose}$	$\mathcal{L}_{obj}$	$\mathcal{L}_{sep}$
	0.4323 ± 0.1671	0.1048 ± 0.0476	0.0029 ± 0.0050	0 ± 0

Table 5.6: Benchmarking results of DON informed KeypointNet with autopicked labels.

The Table 5.7 describes the single class generalized object labels autonomously picked by the KeypointNet from the dense descriptor image. The policy π assigns a random priority to store the labels for 'Suzanne' offline. The labels are queried from the descriptor space using 8 keypoints regressed by the KeypointNet with the seperation margin $\delta = 10$ in pixel space.

Autosampled single class generalized object label	
π(Priority)	Label
1	$[-3.3778, -3.2668, 6.2417]^T$
2	$[-3.4086, -3.3175, 6.2570]^T$
3	$[-3.3793, -3.3144, 6.2799]^T$
4	$[-3.4003, -3.3314, 6.2663]^T$
5	$[-3.3072, -3.1737, 6.1999]^T$
6	$[-3.2575, -3.1253, 6.2076]^T$
7	$[-3.3644, -3.2777, 6.2714]^T$
8	$[-3.3931, -3.2843, 6.2413]^T$

Table 5.7: KeypointNet sampled class generalized labels for 'Suzanne'.

5.3.3 Mining Dense Object Nets Representations in KeypointNet

The KeypointNet is trained to regress 256 keypoints with $\delta = 2$ using ResNet-34 architecture with the same training setting to benchmark the KeypointNet. The upsampled dense output feature dimension is reduced to $D = 16$ for comparing with the DON whose descriptor dimension is set to $D = 16$.

The dense representation put forth by the upsampled dense output feature layer is benchmarked against *PCK@* as in Equation 4.15 in page 17, the same benchmarking process for DON. The upsampled dense output feature evaluates to $AUC \pm \sigma \; for \; PCK@k, \forall k \in [1, 100] = 0.9759 \pm 0.0051$. This result inlines with the DON bechmarked against pixel-wise nt-xent loss with descriptor dimension $D = 16$. Futhermore, the loss for predicting the keypoints increased as illustrated in Figure 5.2 in page 35 as the upsampled dense

output feature dimension is reduced from 256 to 16.

Figure 5.2: Errors in keypoints predictions from KeypointNet modified to benchmark against DON representations.

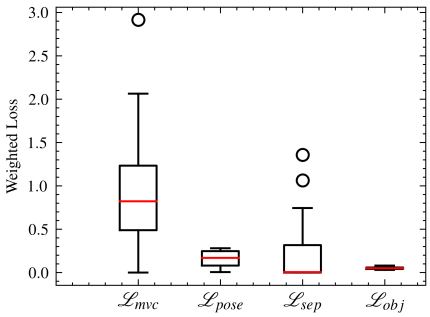

To represent the descriptor space image of dimension $D = 16$ in an image as in Figure 5.3, PCA is used to reduce the dimension to a higher dimensional sub-space of $D = 3$ (a higher dimensional sub-space is the lower dimensional representation of a higher dimension). PCA is only used for visualization purposes. The representation is not consistent as PCA preserves variance in the data while projecting it to a higher dimensional sub-space explaining the ears of 'Suzanne' with same color. No further attempts are carried out to represent dense descriptor images in an image as it does not align with the thesis objective.

Figure 5.3: Depiction of dense descriptors extracted from KeypointNet.

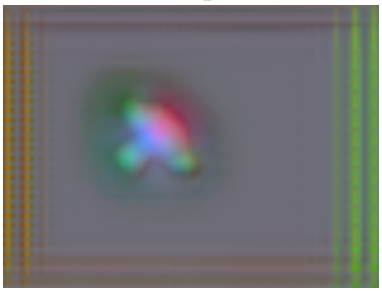

5.4 Generalizing "Caps"

5.4.1 Semantic Correspondence Mapping Pipeline

KeypointNet is trained to predict 100 keypoints with pixel spacing margin $\delta = 5$. Adam optimizer is used to train the network for 1000 epochs with a learning rate 1×10^{-3} and no weight regularization. The W is set similarly to the same value as in the KeypointNet

benchmarking. Furthermore, Keypointnet is based on ResNet-34 architecture with upsampled dense output dimension set to 256.

The KeypointNet is benchmarked for its loss function as detailed in Table 5.8 in page 36. The benchmarking yields higher errors compared to the results in Table 5.4 in page 32 as the number of correspondences is higher and semantically equivalent objects are trained. For the visual inspection purposes, 8 keypoints are sampled randomly as in the Table 5.9 in page 36. Most of the keypoints are semantically well placed, with a few keypoints regressed with high multiview consistent errors.

Semantic Correspondence Mapping Pipeline Benchmarking			
$\mathcal{L}_{mc}$	$\mathcal{L}_{pose}$	$\mathcal{L}_{obj}$	$\mathcal{L}_{sep}$
5.1342 ± 2.8517	0.1456 ± 0.0628	0.2135 ± 0.0771	2.0256 ± 1.2637

Table 5.8: Benchmarking: KeypointNet used for mapping semantic correspondences.

Visual Inspection of Semantic Correspondences		
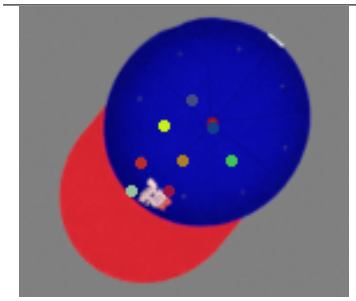	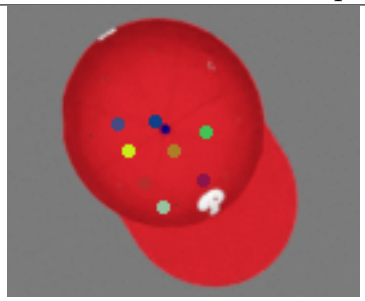	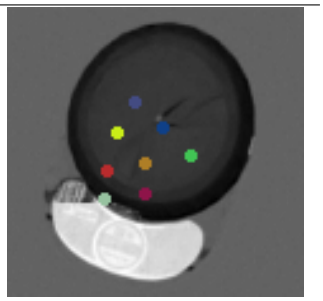

Table 5.9: Illustration of semantic correspondences. The semantic correspondences are color coded.

Furthermore, the semantic correspondence pipeline is examined for the root cause of the high errors. The semantic correspondence pipeline did not converge for a cap in the synthetic dataset. As illustrated in Figure 5.4 in page 37, the keypoints do not meet the properties of geometrically consistent keypoints further, explaining the high errors in Table 5.8 in page 36. The object is removed from the dataset, and the semantic correspondence pipeline is trained again to resolve predictions of keypoints with errors. The errors decrease after another training as seen in Table 5.10 in page 37.

5.4.2 Evaluating Single Class Generalized Labels in the Wild

Two images of caps were collected using a smartphone with a camera to benchmark single-label generalizing ability in the wild as illustrated in Table 5.11 in page 37. Furthermore, from now on, benchmarking method initially used to quantify the neural network

Figure 5.4: Non-Convergence in Semantic Correspondence Pipeline.

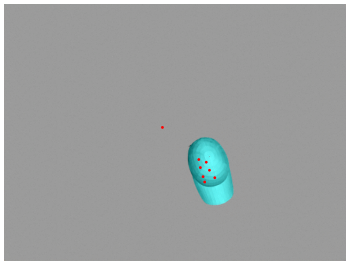

Revised Semantic Correspondence Mapping Pipeline Benchmarking			
$\mathcal{L}_{mc}$	$\mathcal{L}_{pose}$	$\mathcal{L}_{obj}$	$\mathcal{L}_{sep}$
2.1210 ± 1.5937	0.0754 ± 0.1840	0.0780 ± 0.0079	0.1374 ± 1.8752

Table 5.10: Revised bechmarking for semantic correspondences mapping pipeline.

tasks will not be used.

Caps in the Facility	
	

Table 5.11: Depiction of two caps found in the facility.

For evaluating DON trained on the synthetic dataset of caps, DON is trained with ResNet-34 architecture with pixelwise correspondence loss with the dense descriptor dimension $D = 3$ as it is previously found to be performing optimally as can be seen in Table 5.1 in page 30 and computationally economical. Additionally, DON is trained on the semantic correspondences supplied from the KeypointNet, and ADAM optimizer is used with a learning rate of 3×10^{-5} with weight regularization set to 1×10^{-4} for 100 epochs with batch size 2.

The trained DON is tested on the cap images. Judging from Figure 5.5, the descriptors are not placed semantically well. The heatmaps in the image describe a descriptor's

spatial probability in two images. The heatmaps are generated from the interactive application developed to generate robot grasps manually with the temperature parameter set to $t = -0.3$ in Gaussian kernel search space Equation 4.21 in page 19.

Figure 5.5: Testing optimal descriptor placement for the caps in the wild.

Furthermore, the DON is testing using interactive application on the synthetic dataset. As illustrated in the Figure 5.6 in page 38, the DON performs optimally. The DON places spatially optimal descriptors semantically across the objects in the same class.

Figure 5.6: DON performing optimally on the synthetic dataset

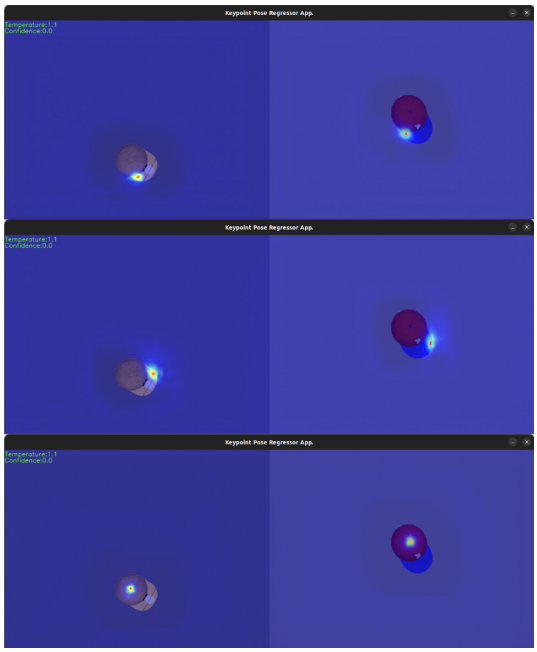

The synthetic dataset is perfect without any faults compared to the real-world data. Despite using background randomizations, noisy backgrounds, colour jitters and greyscaling augmentations, the DON performs poorly on the real-world data as the descriptors are not placed spatially optimally in the semantically same objects.

5.4.3 *"Not losing hope on the real world"*

As per the results, the neural networks perform optimally locally in synthetic data and not real data, further posing an issue for robot grasping.

The neural network implementation scheme has three parts i.e., semantic correspondence mapping pipeline, DON and KeypointNet to pick auto labels. As the semantic correspondence pipeline is noisy and converged with errors as highlighted in Table 5.10 in page 37, the method of generating synthetic correspondences are adopted from [33] to train DON. Furthermore, the DON informed KeypointNet is adapted to regress three keypoints on DON representations generating geometrically consistent 6D poses.

To compute synthetic correspondences, the spatial grid $\mathcal{G}$ as in Equation 4.38 in page 23 is stacked with the RGB image such that the image dimension is as follows:

$$I \rightarrow \mathbb{R}^{H \times W \times \mathbf{5}} \tag{5.1}$$

Furthermore, the image is affinely augmented with previously used augmentations from the vision library provided by [60]. Correspondences are the intersection of the spatial grid in the augmented image and the anchor image as illustrated in the Figure 5.7 in page 39. These synthetic correspondences are further consumed to train DON.

Figure 5.7: Illustrations of synthetic correspondences computed from the image augmentation. The pixel annotated in blue in the left image corresponds to the same pixel annotated in green in the right image.

The synthetic correspondences generalize caps in the real world pretty well, as depicted in the Figure 5.8 in page 5.8.

Figure 5.8: Visual inspection of DON trained on synthetic correspondences.

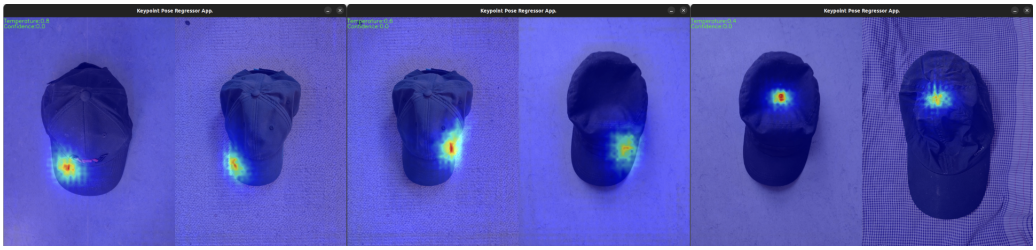

5.4.4 Robot Grasping Pipeline

The KeypointNet is trained on the DON representations to regress 3 geometrically consistent keypoints on dense descriptor images. These keypoint locations are the location of the dense descriptor labels. Furthermore, these labels are stored offline in the .json format as rendered in the Listing 5.1 in page 40 for querying the descriptors in the real-time application.

```
1   ["cap":{
2           "labels":[
3               [3.1030, -3.4000, 2.9119],
4               [5.2890, -2.5363, -0.7921],
5               [0.0596, -3.8049, 2.1469]
6           ]
7           "priority":[
8               1,
9               2,
10              3
11          ]
12      }
13  ]
```

Listing 5.1: Preview of json file entry of offline stored descriptors.

Both DON and DON informed KeypointNet, networks compute robot grasping poses as described below.

Straight 3D Grasps with DON

As illustrated in Figure 5.9 in page 41, the robot moves to a position to capture the image of the cap. The RGB image is fed into the DON to compute a dense descriptor image. The labels previously stored in .json format are read and extracted based on the priority to produce spatial expectation in the descriptor space. The depth map is further used to project the spatial expectation and depth to camera coordinates for generating straight robot grasps.

Figure 5.9: 3D grasping pipeline.

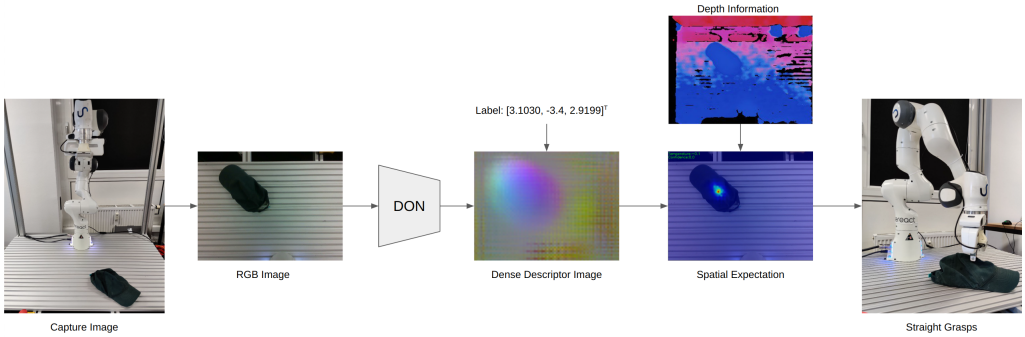

Aligned 6D Grasps with DON Informed KeypointNet

As depicted in Figure 5.10, the robot moves to a position to capture the image of the cap. The RGB image is fed into the DON Informed KeypointNet to compute object 6D pose. The robot realigns the gripper according to the computed object 6D pose and, grasps the object.

Figure 5.10: 6D grasping pipeline.

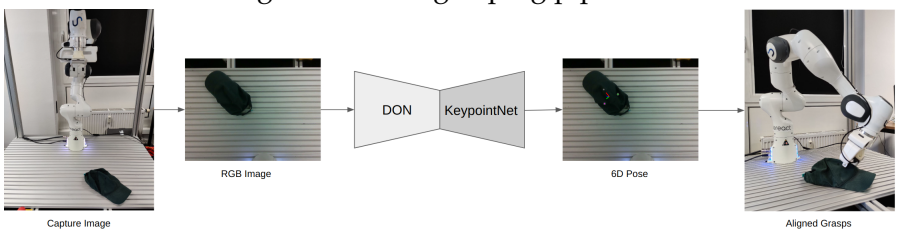

Autonomous Robot Grasping Routine

Figure 5.11 depicts the autonomous robot grasping pipeline. The robot consistently picks the cap robustly using both methods of generating grasps and places the caps aligned, mimicking the industrial robot palletizing routine effectively.

Figure 5.11: Autonomous robot grasping routine.

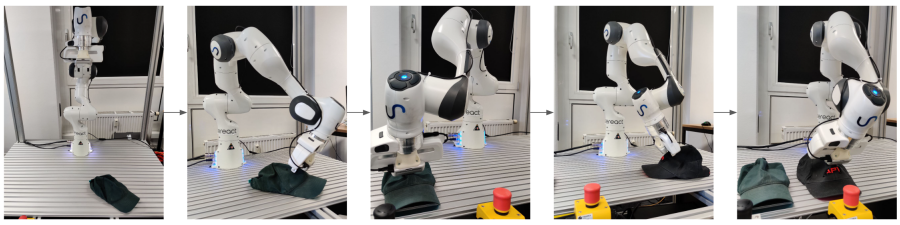

6 Conclusion

The thesis set off with the aim of creating artificial intelligence for robots like Chappie and C-3PO. These robots can perform generalized tasks rather than task-oriented activities, which is the present state of today's artificial intelligence. In particular, the thesis focused on developing generalized representations of an object in an image for robot manipulation solving the present industrial robotics problem of teaching robots to pick every object equipped with 2D or 3D vision systems eliminating the need for explicit programming for each object.

Set on to implement artificial intelligence with generalizing capabilities, DON is implemented. The DON is introduced to the robotics community by Florence *et al.* [9] with generalization capabilities of objects in an image. The DON generates dense descriptor image from an RGB image capable of generalizing an object for robot manipulation. Furthermore, the thesis benchmarked various loss functions, different ResNet neural networks. We have identified that, the "Pixelwise Distribution Loss" with ResNet-34 performs best to generalize objects belonging to the same class (i.e., semantically equivalent) and moreover is computationally economical compared to "Pixelwise NT-Xent Loss". Single class generalized labels manually extracted from the pixels of the dense descriptor image provided by DON are applied to various applications like generating robust object 6D poses of objects in cases of illumination changes, colour changes, occlusion and different viewpoints and other application being robot grasping.

To eliminate the need of manually selecting labels from the dense descriptor image put forth by the DON, KeypointNet is implemented. The KeypointNet, as described, predicts a set of oriented geometrically consistent keypoints on an object such that it preserves the object's 6D pose.

The KeypointNet comes with generalizing properties as it predicts geometrically consistent keypoints across objects belonging to the same class. The generalizing property of KeypointNet is exploited to create a semantic correspondence pipeline to train the DON, replacing the need for depth information which is often noisy with today's technology of depth cameras available. Additionally, the KeypointNet is trained on manifold-based loss making it faster to converge and the need of an orientation network is eliminated. Furthermore, the manifold loss implemented to train the KeypointNet limits the object rotation to a range of $[0, \pi]$. The ResNet-34 architecture performs optimally for the predicting geometrically consistent keypoints. The KeypointNet is sensitive to occlusion

and fails to predict keypoints on occluded areas of objects encountered in the training phase.

As DON is robust against occlusion, KeypointNet could benefit from it. KeypointNet trained on DON representations, regresses a keypoint that occupies a pixel in the dense descriptor image later where this pixel location is queried as a single class generalized label eliminating any need for human intervention.

The upsampled dense output put forth by the KeypointNet represents dense object representations as an alternative to DON to create single-class generalized labels. This ushers an idea that there are other networks capable of computing dense descriptors image similarly to DON.

Initially, the networks are trained on synthetic data. The synthetic data is too perfect to be generalized on real-world objects. The KeypointNet and DON trained on the synthetic dataset did not perform well in the wild. The end-to-end training of neural networks showed reduced performance when trained with the synthetic dataset.

Synthetic correspondences introduced in [33] are used to overcome the limitations of training the networks posed by the synthetic data. The synthetic correspondences are independent of camera intrinsic and extrinsic information, including depth information to compute correspondences. The DON is trained on images of caps captured from a smartphone with a camera with synthetic correspondence and performed well, generalizing most of the caps in the wild.

The capabilities of DON and KeypointNet are demonstrated and applied to generalized autonomous robot task of cap pick-and-place operation.

7 Future Scope

As the Keypointnet is limited by the manifold losses for training objects with rotation in range $[0, \pi]$, a newer formulation will be engineered and applied. Furthermore, KeypointNet and DON will be expanded to accommodate objects belonging to different classes.

As of this writing, the DON training cannot accommodate multiple similar object in an image as it is limited by the presented loss functions [30, 33]. To overcome this, "Ranked InfoNCE Loss" [61] will be adopted on the pixelwise scale to train DON accommodating multiple similar objects in a scene.

To build up appropriate states for the future robot path planning and grasping using model-based reinforcement learning [62], DON computed dense descriptor image will be encoded to a vector state $x \in \mathbb{R}^D$ instead of $I_D \in \mathbb{R}^{H \times W \times D}$ with the neural networks inspired from [63] for faster online training. The robot path planning will be based on the KeypointNet alternatively to the method trajectory generation proposed in [12].

Bibliography

[1] *Sereact*, "AI Robots for Production. Today". https://sereact.ai/en.

[2] D. Silver, T. Hubert, J. Schrittwieser, I. Antonoglou, M. Lai, A. Guez, M. Lanctot, L. Sifre, D. Kumaran, T. Graepel, *et al.*, "A general reinforcement learning algorithm that masters chess, shogi, and go through self-play", *Science*, vol. 362, no. 6419, pp. 1140–1144, 2018.

[3] D. Silver, A. Huang, C. J. Maddison, A. Guez, L. Sifre, G. Van Den Driessche, J. Schrittwieser, I. Antonoglou, V. Panneershelvam, M. Lanctot, *et al.*, "Mastering the game of go with deep neural networks and tree search", *nature*, vol. 529, no. 7587, pp. 484–489, 2016.

[4] A. Krizhevsky, I. Sutskever, and G. E. Hinton, "Imagenet classification with deep convolutional neural networks", *Communications of the ACM*, vol. 60, no. 6, pp. 84–90, 2017.

[5] J. Long, E. Shelhamer, and T. Darrell, "Fully convolutional networks for semantic segmentation", in *Proceedings of the IEEE conference on computer vision and pattern recognition*, 2015, pp. 3431–3440.

[6] K. He, G. Gkioxari, P. Dollár, and R. Girshick, "Mask r-cnn", in *Proceedings of the IEEE international conference on computer vision*, 2017, pp. 2961–2969.

[7] R. A. Güler, N. Neverova, and I. Kokkinos, "Densepose: Dense human pose estimation in the wild", in *Proceedings of the IEEE conference on computer vision and pattern recognition*, 2018, pp. 7297–7306.

[8] R. Anyoha, "The history of artificial intelligence.", Available at https://sitn.hms.harvard.edu/flash/2017/history-artificial-intelligence/.

[9] P. R. Florence, L. Manuelli, and R. Tedrake, "Dense object nets: Learning dense visual object descriptors by and for robotic manipulation", *arXiv preprint arXiv:1806.08756*, 2018.

[10] P. Sundaresan, J. Grannen, B. Thananjeyan, A. Balakrishna, M. Laskey, K. Stone, J. E. Gonzalez, and K. Goldberg, "Learning rope manipulation policies using dense object descriptors trained on synthetic depth data", *CoRR*, vol. abs/2003.01835, 2020. arXiv: 2003.01835.

[11] C.-Y. Chai, K.-F. Hsu, and S.-L. Tsao, "Multi-step pick-and-place tasks using object-centric dense correspondences", in *2019 IEEE/RSJ International Conference on Intelligent Robots and Systems (IROS)*, 2019, pp. 4004–4011.

[12] P. Florence, L. Manuelli, and R. Tedrake, "Self-supervised correspondence in visuomotor policy learning", *IEEE Robotics and Automation Letters*, vol. 5, no. 2, pp. 492–499, 2019.

[13] A. Ganapathi, P. Sundaresan, B. Thananjeyan, *et al.*, "Learning dense visual correspondences in simulation to smooth and fold real fabrics", in *2021 IEEE International Conference on Robotics and Automation (ICRA)*, 2021, pp. 11 515–11 522.

[14] A. Kupcsik, M. Spies, A. Klein, M. Todescato, N. Waniek, P. Schillinger, and M. Bürger, "Supervised training of dense object nets using optimal descriptors for industrial robotic applications", *arXiv preprint arXiv:2102.08096*, 2021.

[15] B. Pal, S. Khaiyum, and Y. S. Kumaraswamy, "3d point cloud generation from 2d depth camera images using successive triangulation", in *2017 International Conference on Innovative Mechanisms for Industry Applications (ICIMIA)*, 2017, pp. 129–133.

[16] Y. Song and H. Yan, "Image segmentation techniques overview", in *2017 Asia Modelling Symposium (AMS)*, 2017, pp. 103–107.

[17] S. Noor, M. Waqas, M. I. Saleem, and H. N. Minhas, "Automatic object tracking and segmentation using unsupervised siammask", *IEEE Access*, vol. 9, pp. 106 550–106 559, 2021.

[18] A. Maćkiewicz and W. Ratajczak, "Principal components analysis (pca)", *Computers & Geosciences*, vol. 19, no. 3, pp. 303–342, 1993.

[19] V. Klema and A. Laub, "The singular value decomposition: Its computation and some applications", *IEEE Transactions on Automatic Control*, vol. 25, no. 2, pp. 164–176, 1980.

[20] S. Ruder, "An overview of multi-task learning in deep neural networks", *CoRR*, vol. abs/1706.05098, 2017. arXiv: 1706.05098.

[21] S. Suwajanakorn, N. Snavely, J. J. Tompson, and M. Norouzi, "Discovery of latent 3d keypoints via end-to-end geometric reasoning", *Advances in neural information processing systems*, vol. 31, 2018.

[22] T. Schmidt, R. Newcombe, and D. Fox, "Self-supervised visual descriptor learning for dense correspondence", *IEEE Robotics and Automation Letters*, vol. 2, no. 2, pp. 420–427, 2016.

[23] D. G. Lowe, "Object recognition from local scale-invariant features", in *Proceedings of the seventh IEEE international conference on computer vision*, Ieee, vol. 2, 1999, pp. 1150–1157.

[24] X. Zhao, R. Vemulapalli, P. A. Mansfield, B. Gong, B. Green, L. Shapira, and Y. Wu, "Contrastive learning for label efficient semantic segmentation", in *Proceedings of the IEEE/CVF International Conference on Computer Vision*, 2021, pp. 10 623–10 633.

[25] J. Fedoruk, B. Schmuland, J. Johnson, and G. Heo, "Dimensionality reduction via the johnson–lindenstrauss lemma: Theoretical and empirical bounds on embedding dimension", *The Journal of Supercomputing*, vol. 74, no. 8, pp. 3933–3949, 2018.

[26] L. Van der Maaten and G. Hinton, "Visualizing data using t-sne.", *Journal of machine learning research*, vol. 9, no. 11, 2008.

[27] M. Belkin and P. Niyogi, "Laplacian eigenmaps for dimensionality reduction and data representation", *Neural computation*, vol. 15, no. 6, pp. 1373–1396, 2003.

[28] R. Hartley and A. Zisserman, *Multiple view geometry in computer vision*. Cambridge university press, 2003.

[29] D. Hadjivelichkov and D. Kanoulas, "Fully self-supervised class awareness in dense object descriptors", in *5th Annual Conference on Robot Learning*, 2021.

[30] P. R. Florence, "Dense visual learning for robot manipulation", Ph.D. dissertation, Massachusetts Institute of Technology, 2020.

[31] T. Chen, S. Kornblith, M. Norouzi, and G. Hinton, "A simple framework for contrastive learning of visual representations", in *International conference on machine learning*, PMLR, 2020, pp. 1597–1607.

[32] J. Zbontar, L. Jing, I. Misra, Y. LeCun, and S. Deny, "Barlow twins: Self-supervised learning via redundancy reduction", in *International Conference on Machine Learning*, PMLR, 2021, pp. 12 310–12 320.

[33] D. B. Adrian, A. G. Kupcsik, M. Spies, and H. Neumann, "Efficient and robust training of dense object nets for multi-object robot manipulation", in *2022 International Conference on Robotics and Automation (ICRA)*, IEEE, 2022, pp. 1562–1568.

[34] C.-Y. Chai, K.-F. Hsu, and S.-L. Tsao, "Multi-step pick-and-place tasks using object-centric dense correspondences", in *2019 IEEE/RSJ International Conference on Intelligent Robots and Systems (IROS)*, IEEE, 2019, pp. 4004–4011.

[35] M. E. Fathy, Q.-H. Tran, M. Z. Zia, P. Vernaza, and M. Chandraker, "Hierarchical metric learning and matching for 2d and 3d geometric correspondences", in *Proceedings of the european conference on computer vision (ECCV)*, 2018, pp. 803–819.

[36] L. Yen-Chen, P. Florence, J. T. Barron, T.-Y. Lin, A. Rodriguez, and P. Isola, *Nerf-supervision: Learning dense object descriptors from neural radiance fields*, 2022.

[37] B. Mildenhall, P. P. Srinivasan, M. Tancik, J. T. Barron, R. Ramamoorthi, and R. Ng, "Nerf: Representing scenes as neural radiance fields for view synthesis", *Communications of the ACM*, vol. 65, no. 1, pp. 99–106, 2021.

[38] L. Manuelli, W. Gao, P. R. Florence, and R. Tedrake, "Kpam: Keypoint affordances for category-level robotic manipulation", *CoRR*, vol. abs/1903.06684, 2019. arXiv: 1903.06684.

[39] M. Vecerik, J.-B. Regli, O. Sushkov, D. Barker, R. Pevceviciute, T. Rothörl, C. Schuster, R. Hadsell, L. Agapito, and J. Scholz, "S3k: Self-supervised semantic keypoints for robotic manipulation via multi-view consistency", *arXiv preprint arXiv:2009.14711*, 2020.

[40] L. Yen-Chen, A. Zeng, S. Song, P. Isola, and T.-Y. Lin, "Learning to see before learning to act: Visual pre-training for manipulation", in *2020 IEEE International Conference on Robotics and Automation (ICRA)*, IEEE, 2020, pp. 7286–7293.

[41] P. Sermanet, C. Lynch, J. Hsu, and S. Levine, "Time-contrastive networks: Self-supervised learning from multi-view observation", in *2017 IEEE Conference on Computer Vision and Pattern Recognition Workshops (CVPRW)*, IEEE, 2017, pp. 486–487.

[42] Y. Li, G. Wang, X. Ji, Y. Xiang, and D. Fox, "Deepim: Deep iterative matching for 6d pose estimation", in *Proceedings of the European Conference on Computer Vision (ECCV)*, 2018, pp. 683–698.

[43] Y. Xiang, T. Schmidt, V. Narayanan, and D. Fox, "Posecnn: A convolutional neural network for 6d object pose estimation in cluttered scenes", *arXiv preprint arXiv:1711.00199*, 2017.

[44] A. X. Chang, T. Funkhouser, L. Guibas, P. Hanrahan, Q. Huang, Z. Li, S. Savarese, M. Savva, S. Song, H. Su, *et al.*, "Shapenet: An information-rich 3d model repository", *arXiv preprint arXiv:1512.03012*, 2015.

[45] A. Simeonov, Y. Du, A. Tagliasacchi, J. B. Tenenbaum, A. Rodriguez, P. Agrawal, and V. Sitzmann, *Neural descriptor fields: Se(3)-equivariant object representations for manipulation*, 2021.

[46] K. He, X. Zhang, S. Ren, and J. Sun, "Deep residual learning for image recognition", pp. 770–778, 2016.

[47] S. I. Nikolenko, *Synthetic data for deep learning*. Springer, 2021, vol. 174.

[48] T. Chen, S. Kornblith, M. Norouzi, and G. Hinton, "A simple framework for contrastive learning of visual representations", in *International conference on machine learning*, PMLR, 2020, pp. 1597–1607.

[49] A. v. d. Oord, Y. Li, and O. Vinyals, "Representation learning with contrastive predictive coding", *arXiv preprint arXiv:1807.03748*, 2018.

[50] C.-Y. Chai, K.-F. Hsu, and S.-L. Tsao, "Multi-step pick-and-place tasks using object-centric dense correspondences", in *2019 IEEE/RSJ International Conference on Intelligent Robots and Systems (IROS)*, IEEE, 2019, pp. 4004–4011.

[51] M. Denninger, M. Sundermeyer, D. Winkelbauer, Y. Zidan, D. Olefir, M. Elbadrawy, A. Lodhi, and H. Katam, "Blenderproc", *arXiv preprint arXiv:1911.01911*, 2019.

[52] S. Kelly, "Basic introduction to pygame", in *Python, PyGame and Raspberry Pi Game Development*, Springer, 2016, pp. 59–65.

[53] R. Bhatia, *Matrix analysis*. Springer Science & Business Media, 2013, vol. 169.

[54] D. Q. Huynh, "Metrics for 3d rotations: Comparison and analysis", *Journal of Mathematical Imaging and Vision*, vol. 35, no. 2, pp. 155–164, 2009.

[55] J. M. Lee, *Introduction to Riemannian manifolds*. Springer, 2018, vol. 176.

[56] W. Kabsch, "A solution for the best rotation to relate two sets of vectors", *Acta Crystallographica Section A: Crystal Physics, Diffraction, Theoretical and General Crystallography*, vol. 32, no. 5, pp. 922–923, 1976.

[57] C. B. Choy, J. Gwak, S. Savarese, and M. Chandraker, "Universal correspondence network", *Advances in neural information processing systems*, vol. 29, 2016.

[58] S. Levine, C. Finn, T. Darrell, and P. Abbeel, "End-to-end training of deep visuomotor policies", *The Journal of Machine Learning Research*, vol. 17, no. 1, pp. 1334–1373, 2016.

[59] D. P. Kingma and J. Ba, "Adam: A method for stochastic optimization", *arXiv preprint arXiv:1412.6980*, 2014.

[60] A. Paszke, S. Gross, F. Massa, A. Lerer, J. Bradbury, G. Chanan, T. Killeen, Z. Lin, N. Gimelshein, L. Antiga, *et al.*, "Pytorch: An imperative style, high-performance deep learning library", *Advances in neural information processing systems*, vol. 32, 2019.

[61] D. T. Hoffmann, N. Behrmann, J. Gall, T. Brox, and M. Noroozi, "Ranking info noise contrastive estimation: Boosting contrastive learning via ranked positives", in *AAAI Conference on Artificial Intelligence*, 2022.

[62] L. Kaiser, M. Babaeizadeh, P. Milos, B. Osinski, R. H. Campbell, K. Czechowski, D. Erhan, C. Finn, P. Kozakowski, S. Levine, *et al.*, "Model-based reinforcement learning for atari", *arXiv preprint arXiv:1903.00374*, 2019.

[63] M. Tschannen, O. Bachem, and M. Lucic, "Recent advances in autoencoder-based representation learning", *arXiv preprint arXiv:1812.05069*, 2018.

List of Acronyms

RGB	3-Channel Image
RGB-D	4-Dimensional Image, i.e., RGB with Depth
CNN	Convolutional Neural Network
DL	Deep Learning
DNN	Deep Neural Network
DON	Dense Object Nets
NeRF	Neural Radiance Fields
PCA	Principal Component Analysis
ResNet	Residual Network
s.t.	such that
SIFT	Scale-Invariant Feature Transform
SVD	Singular Value Decomposition
SOTA	State of the Art

List of Figures

4.1 DON architecture. 13
4.2 2D spatial expectation of keypoint in two images. 16
4.3 Variance loss function at work. 23
4.4 KeypointNet Architecture. 26
4.5 The image in the right illustrates the noisy backgrounds and the image in left describes random background augmentation. 27
4.6 Robot setup for cap grasping with wrist-mounted camera. 28

5.1 Output of trained ResNet-34 for KeypointNet task. 32
5.2 Errors in keypoints predictions from KeypointNet modified to benchmark against DON representations. 35
5.3 Depiction of dense descriptors extracted from KeypointNet. 35
5.4 Non-Convergence in Semantic Correspondence Pipeline. 37
5.5 Testing optimal descriptor placement for the caps in the wild. 38
5.6 DON performing optimally on the synthetic dataset 38
5.7 Illustrations of synthetic correspondences computed from the image augmentation. The pixel annotated in blue in the left image corresponds to the same pixel annotated in green in the right image. 39
5.8 Visual inspection of DON trained on synthetic correspondences. 40
5.9 3D grasping pipeline. 41
5.10 6D grasping pipeline. 41
5.11 Autonomous robot grasping routine. 41

List of Tables

2.1 Comparison of influential SOTA. 11

4.1 Depiction of dataset quintennsials features of dataset 18
4.2 Illustration of caps sampled from the Shapenet library [44]. 26

5.1 DON evaluation against $AUC \pm \sigma \; for \; PCK@K$ metric. 30
5.2 Visual inspection for optimal placement of descriptors. 31
5.3 Testing descriptors for robost 6D pose generation. 31
5.4 Benchmarking KeypointNet with individual losses. 32
5.5 Benchmarking KeypointNet informed DON for their individual performance. 33
5.6 Benchmarking results of DON informed KeypointNet with autopicked labels. 34
5.7 KeypointNet sampled class generalized labels for 'Suzanne'. 34
5.8 Benchmarking: KeypointNet used for mapping semantic correspondences. 36
5.9 Illustration of semantic correspondences. The semantic correspondences are color coded. 36
5.10 Revised bechmarking for semantic correspondences mapping pipeline. . 37
5.11 Depiction of two caps found in the facility. 37

Listings

5.1 Preview of json file entry of offline stored descriptors. 40

List of Symbols

Symbol	Description
$\mathbf{D}$	Dense descriptor dimension
$\mathbb{N}^+$	Set of positive integers
$\in$	Belongs to or in
$\mathcal{M}$	Riemannian manifold
$SO(n)$	Special orthogonal group of dimension n
$SE(3)$	Special euclidean group of dimension 3
$\mathbb{R}^n$	Real number of dimension n
$\langle \cdot , \cdot \rangle$	Scalar product of two vectors
$\| \cdot \|$	L^2 Norm
$\| \cdot \|_F$	Frobenius Norm